Hemin-binding DNA structures on the surface of bacteria promote extracellular electron transfer

*Obinna M. Ajunwa[1], Gabriel Antonio S. Minero[1], Sissel D. Jensen[1], Rikke L. Meyer[1,2]**

[1] Interdisciplinary Nanoscience Center (iNANO), Aarhus University, Gustav Wieds Vej 14, 8000 Aarhus, Denmark
[2] Department of Biology, Aarhus University, Ny Munkegade 114, 8000 Aarhus, Denmark
*Corresponding author: rikke.meyer@inano.au.dk

ABSTRACT

Recent research has shown that bacteria in anoxic layers of *Pseudomonas aeruginosa* biofilms can respire by transferring electrons to oxygen via extracellular DNA (eDNA) and DNA-binding redox mediators that are unique to this species[1]. In this study, we propose a similar but generic mechanism by which bacteria can transfer electrons via DNA in biofilms, using hemin as a redox-mediator and hemin-binding G-quadruplex (G4) DNA structures in the extracellular matrix.

Using *Staphylococcus epidermidis* as a model organism, voltammetry showed that eDNA and hemin were needed for extracellular electron transfer (EET). Surface-associated G4-DNA formed a complex with hemin, which transferred electrons from the bacteria to an electrode under anoxic conditions. Addition of G4-DNA and hemin to growing biofilms promoted EET which was stable for days. G4-DNA/hemin is also a peroxidase-like DNAzyme, capable of transferring electrons from bacteria to H_2O_2.

G4-DNA were only recently discovered to be abundant in the extracellular matrix of biofilms[2,3]. We now show that hemin turns these structures into conduits for EET. The study opens the door to new and generic mechanisms for bacterial energy conservation under oxygen-limiting conditions, and for tackling H_2O_2, a common host defense mechanism against bacterial infections.

Keywords: *Extracellular electron transfer; G-quadruplex; hemin; eDNA; biofilm*

INTRODUCTION

Bacterial electroactivity describes a process by which bacteria use extracellular electron transfer (EET) to move electrons to or from metabolic processes in the cell[4,5]. This concept was previously thought to occur in a few prokaryotes that contain organelles or produce specific redox mediators[6]. However, a new report suggests that EET might be a ubiquitous phenomenon among microorganisms[7].

EET is particularly beneficial for bacteria that use solid electron acceptors or that live in steep chemical gradients where soluble electron acceptors are out of reach. Biofilms create such gradients by consuming oxygen, and bacteria in the anoxic layers can benefit from using EET to transfer electrons to the oxic layer. In biofilms, bacteria are connected by a matrix of polymeric substances, such as polysaccharides, lipids, peptides, proteins and nucleic acids. Several of these are conductive and have been implicated in EET, e.g. polysaccharides in *Geobacter sulfurreducens*[8] and polypeptides in *Bacillus subtilis*[9]. Recently, extracellular DNA (eDNA) was also implicated in EET. *Pseudomonas aeruginosa* transferred electrons from anoxic to oxic layers in biofilms via eDNA and small DNA-binding redox-active molecules called phenazines (pyocyanin and phenazine carboxamide). The soluble phenazines transferred electrons from intracellular metabolic processes to the extracellular "eDNA grid" and subsequently to oxygen[1].

This mechanism for EET is unique to the pyocyanin-producing *P. aeruginosa*. However, DNA is a common biofilm component, and we therefore wondered if a similar but more generic principle for EET exists, where DNA-binding redox-active molecules transfer electrons from bacteria to a conductive eDNA network. We and others recently showed that eDNA and eRNA in biofilms can contain a variety of secondary structures: Z-DNA, i-motifs and G-quadruplexes (G4-DNA)[2,3,10,11], and these are scattered throughout a net-like DNA superstructure in the biofilm's extracellular matrix. The planar guanine quartets of G4-DNA have an increased potential for π-stacking and electron orbital sharing[12], which leads it to form a stable complex with hemin – one of the most abundant redox mediators in biology. The G4-DNA/hemin complex is also a DNAzyme with oxidoreductase activity. We hypothesized that G4-DNA/hemin complexes can facilitate EET in biofilms, and that this is a generic mechanism for DNA-mediated EET.

The aim of this study was to provide proof-of-concept for G4-DNA/hemin-mediated EET in bacteria, and to demonstrate how these structures can boost EET in biofilms. We first determined if G4-DNA/hemin could interact with bacteria and facilitate EET. We then characterized the electrochemical signatures and charge transfer mediated by G4-DNA/hemin associated with both planktonic bacteria and biofilms of *S. epidermidis*. *S. epidermidis* is one of the most common culprits of implant-associated infections, and its main virulence factor is the ability to form biofilms. We used *S. epidermidis* as the model organism in this study due to its clinical relevance and because it was previously reported to produce large amounts of eDNA in the biofilm matrix – including G4-DNA structures[3].

Our results support a scenario by which G4-DNA/hemin complexes associate with extracellular DNA and support bacterial metabolism through EET. With this knowledge, we believe that EET may provide a mechanism for bacteria in biofilms to sustain metabolic activity by long-range transfer of electrons to oxygen or hydrogen peroxide in the infectious microenvironment.

RESULTS

S. epidermidis can interact electrochemically with hemin via extracellular DNA (eDNA)

Our first aim was to establish if eDNA and hemin can confer electrochemical activity in *S. epidermidis* biofilms. We used voltammetry to compare the electrochemical signatures of biofilms with high and low amounts of eDNA. Biofilms of *S. epidermidis* 1457 wildtype or an eDNA-deficient strain (*S. epidermidis* 1457 Δ*atlE)* grew directly on the surface of electrodes for 48 h in media with hemin, and voltammograms (DPV and CV) confirmed a difference between the strains (Fig. 1 and extended Data Fig. 1). In CV analyses, the wildtype strain produced slight oxidation peaks at -0.10 V and +0.33 V and reduction peaks at -0.23 V and -0.37 V, but these peaks were not as distinct in the eDNA-deficient mutant strain (Extended Data Fig. 1).

DPV analysis was more sensitive, and sterile controls contained a peak at -0.38 V resulting from dissolved hemin (Fig. 1a). Next, we grew planktonic *S. epidermidis* 1457 in media +/- hemin for 48 h and submerged the electrode to determine if planktonic bacteria could contribute to the electrochemical signal. These planktonic cultures contained no peaks – not even in samples with hemin (Fig. 1a), indicating that the bacteria removed hemin from solution, and that planktonic bacteria did not contribute to the electrochemical signature of biofilms in subsequent experiments.

In contrast to planktonic cultures, we observed two DPV peaks from biofilms grown on the electrode surface for 48 h in media with hemin (Fig. 1a). One peak (at +0.1-0.2 V) most likely represented the biomass, and this peak was independent of hemin in the media. In contrast, a very distinguished peak at -0.25 V was only present in biofilms grown with hemin, and we ascribed this peak to the electrochemical activity of hemin embedded in the biofilm. Importantly, the position of this peak was slightly shifted, relative to the peak from dissolved hemin, indicating that hemin interacts with another component - possibly eDNA.

To test this hypothesis, we conducted the same experiment on *S. epidermidis* 1457 Δ*atlE*, which forms biofilms that contain very little eDNA (Fig. 1b). The DPV peak associated with hemin in the biofilm was much smaller for this sample, which corroborates our hypothesis that hemin interacts with eDNA to confer electrochemical activity in biofilms.

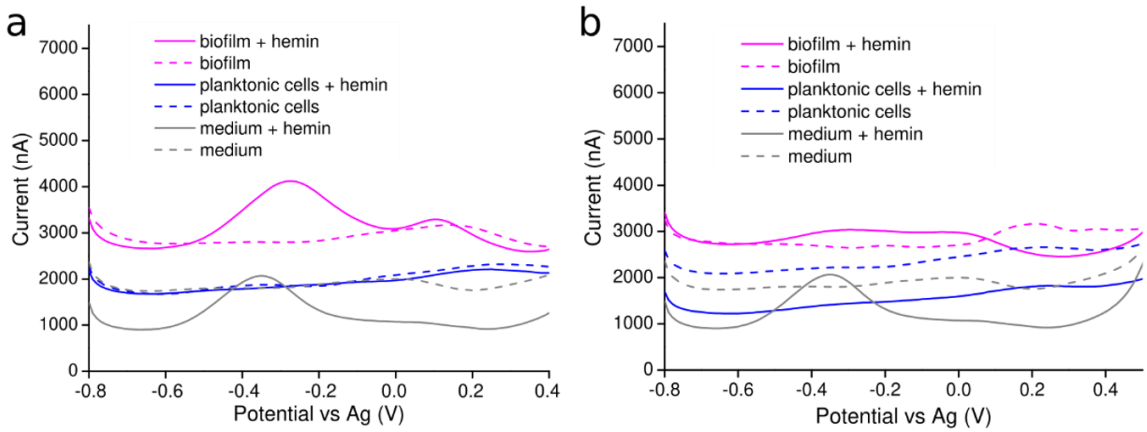

Fig. 1: **eDNA and hemin facilitate electrochemical signature of electroactive biofilms.** Differential Pulse Voltammogram (DPV) of biofilms and planktonic cultures of **a)** *S. epidermidis* 1457 (eDNA producing) and **b)** *S. epidermidis* 1457 Δ*atlE* (non-eDNA producing) grown for 48 h in the presence or absence of 5 µM hemin. DPV curves are averages (n=3). Sterile medium (TSB, 0.2 M NaCl, +/- 5 µM hemin) served as control.

Hemin bound to G-quadruplex DNA can confer extracellular electron transport

We hypothesized that the electrochemical interaction between eDNA and hemin involves G4-DNA/hemin complexes. To test this hypothesis, we generated an experimental model in which *S. epidermidis* was loaded with G4-DNA on the surface, enabling us to study EET in bacteria with or without surface-associated G4-DNA/hemin.

Extracellular DNA co-localizes with exopolysaccharides in biofilms, and we therefore used *S. epidermidis* 1585 pTX*icaADBC*[13] which has inducible production of poly-n-acetyl glucosamine (PNAG) to promote G4-DNA adsorption. We folded two different DNA oligos (c-Myc1 and c-Myc3) into G4-DNA (Extended Data Fig. 2), mixed them with *S. epidermidis*, and visualized surface-associated G4-DNA by fluorescence immunolabeling. We show that G4-DNA adsorbed primarily to PNAG-producing cells (Fig. 2a), and the G4 trimer c-Myc3 absorbed in larger quantity than c-Myc1 (Extended Data Fig. 4), resulting in higher electroactivity (Extended Data Fig. 5). We therefore chose c-Myc3 for our further analyses, and we used *S. epidermidis* 1585 pTX*icaADBC* +/- induction of PNAG production as positive and negative controls for bacteria +/- G4-DNA on the surface. *S. epidermidis* 1585 pTX*icaADBC* was used in all subsequent experiments unless specifically stated.

In an experiment to check that hemin was not toxic to the bacteria, we incubated *S. epidermidis* +/- induction of PNAG production and in the presence/absence of G4-DNA, and presence/absence of 5 µM hemin in the growth media. CFU enumeration of overnight cultures confirmed that hemin was not toxic, but it also revealed a 10-fold increase in CFU in samples with hemin. Notably, this increase in CFU only occurred in cultures with surface-adsorbed G4-DNA (Extended Data Fig. 3). Thus, hemin increased the growth yield when bacteria contained G4-DNA in the cell envelope.

Next, we grew planktonic cultures +/- induction of PNAG, added G4-DNA, hemin, or G4-DNA + hemin, and incubated for 1 h before washing and depositing the bacteria on the electrode surface for quantification of charge transfer at 0.4 V, which would capture the electrochemical potential of eDNA/hemin according to our results in Fig. 1. The charge measured in this experiment depends both on the number of bacteria on the electrode surface, and their ability to transfer electrons. We therefore visualized the adsorbed bacteria and G4-DNA within the adsorbed layer. Both strains adsorbed on the electrode surface as a dense layer, but only the PNAG-producing strain contained G4-DNA (Fig. 2a). Differences in charge transfer could therefore be ascribed to differences in mechanisms for electron transfer rather than differences in biomass.

The total electrical charge measured after short chronoamperometric analysis showed that EET activity was higher for bacteria with G4-DNA and hemin (Fig. 2b). In contrast, the total charge for bacteria incubated with G4-DNA alone was not significantly different from the control. Bacteria incubated with hemin showed a small increase in electrical charge compared to the control, but much less than bacteria incubated with both hemin and G4-DNA. This small charge may be attributed to direct electron transfer via hemin, or by hemin bound to G4-DNA structures naturally present on the bacterial surface. When repeating the experiment on *S. epidermidis* without PNAG induction and therefore unable to adsorb G4-DNA, none of the samples had a higher electrical charge than the control (Fig. 2c), supporting our conclusion that G4-DNA/hemin complexes facilitate electrical charge transfer.

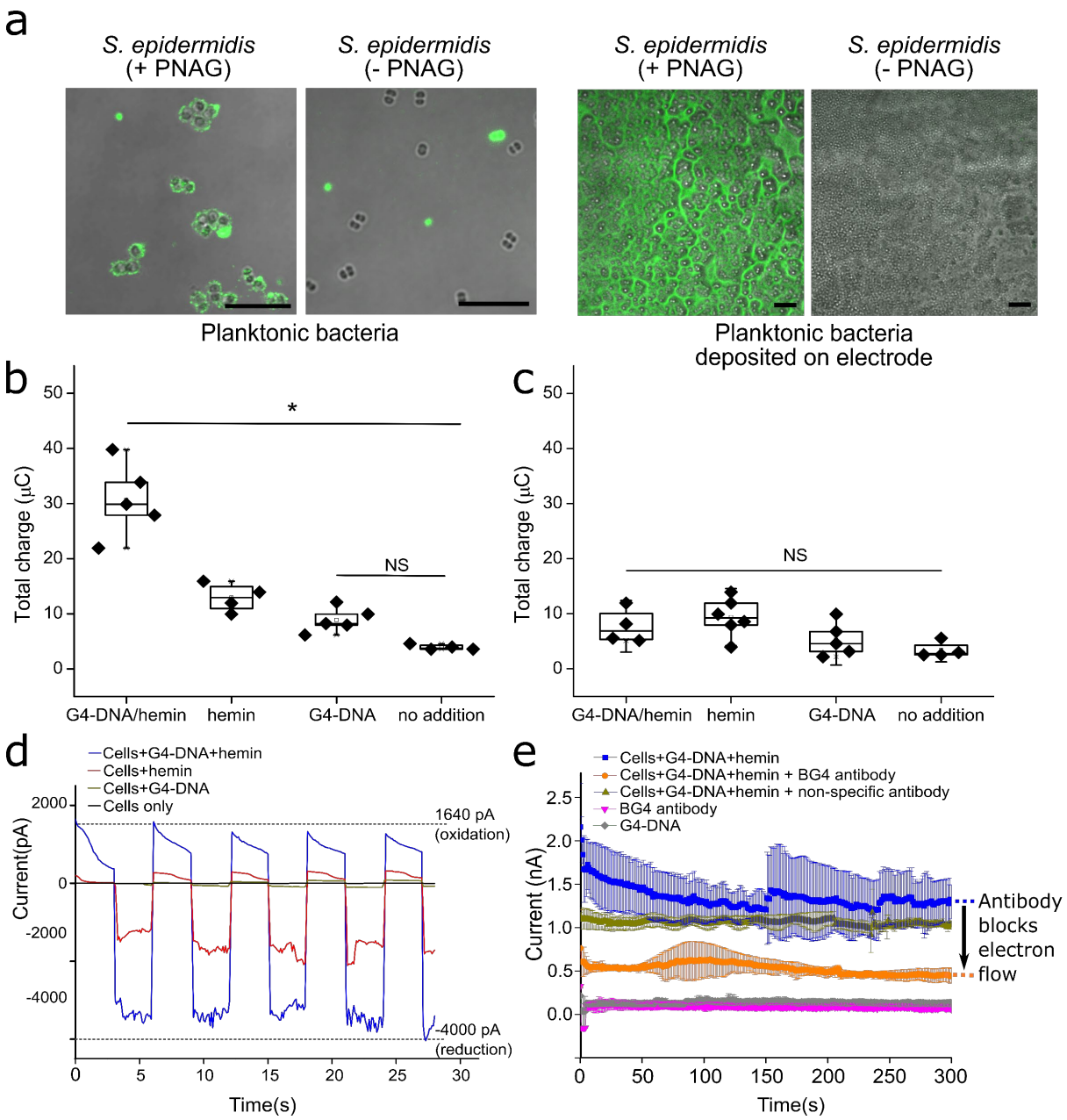

Fig. 2 G4-DNA adsorbs on cell surface of PNAG-producing *S. epidermidis* and enables bidirectional electron flow.

a. Externally added G4-DNA adsorbs to the surface of planktonic *S. epidermidis* if PNAG production is induced. Planktonic *S. epidermidis* were grown ±xylose for PNAG induction and incubated with G4-DNA for 1 h. The bacteria form a dense layer when deposited on an electrode for subsequent analysis (lower panel). Confocal laser scanning (CLSM) images show bacteria (brightfield) and G4-DNA (green) visualized by fluorescence immunolabeling with antibody BG4. Scalebar = 10 µm.

b. Charge transfer from PNAG-induced *S. epidermidis*. Addition of G4-DNA/hemin generated significantly higher total charge after 300 s at 0.4 V poised potential. Hemin did not increase charge transfer if G4-DNA was absent. ∗ represents statistical significance ($p < 0.05$), ANOVA and Tukey's test, NS= Not significant.

c. Charge transfer from PNAG-deficient *S. epidermidis* that do not bind G4-DNA. Addition of G4-DNA and hemin did not affect the total electrical charge.

d. G4-DNA/hemin on the surface of *S. epidermidis* could release and uptake electrons bidirectionally as demonstrated by short multi-step chronoamperometric analyses (MSCA). Values are an averages (n=3).

e. Blocking the contact between G4-DNA/hemin and the electrode surface with G4-specific antibodies disrupts EET. A decline in the electron flow (indicated by black arrow) from planktonic *S. epidermidis* with G4-DNA/hemin was observed after interaction with G4-DNA antibody.

188
189 **G4-DNA/hemin on the bacterial surface enables bi-directional electron flow**
190 EET enables release of electrons from bacteria (electrogenicity) but could be used for electron
191 harvesting (electrotrophy) as reported in electroactive prokaryotes involved in biocorrosion and
192 element cycling[5,14]. The robustness of an EET mechanism can be shown in its ability to
193 facilitate bi-directional electron flow, creating a tool for energy generation through electrical
194 respiration[15]. We therefore sought to determine if G4-DNA/hemin in the bacterial cell envelope
195 could convey bi-directional electron flow.
196 We evaluated the oxidative and reductive electron flow using short-span multi-step
197 chronamperometry (MSCA) under oxidative (0.4 V) and reductive (-0.4 V) potentials, and
198 quantified the current from *S. epidermidis* treated with G4-DNA, hemin, or both. We observed
199 a larger difference in the current when poising the electrode for reduction (electrons flowing
200 from the electrode) compared to oxidation (electrons flowing to the electrode) (Fig. 2d). The
201 electron flow toward the electrode requires electron donors from bacterial metabolism, while
202 electrons are acquired directly from the electrode surface when flowing in the opposite
203 direction. The difference in current may therefore simply reflect the availability of electrons.
204 The difference in reductive and oxidative current was only observed in samples supplemented
205 with hemin, and it was amplified when both hemin and G4-DNA was present. This lends further
206 support to our hypothesis that G4-DNA/hemin complexes promote electron flow.
207
208 **Electron flow requires direct contact between G4-DNA/hemin and the electrode**
209 If the G4-DNA/hemin complex is specifically needed for electron transfer, we expect that G4-
210 DNA/hemin must make direct contact with the electrode to facilitate electron flow. To
211 investigate this, we coated the electrode surface with a G4-DNA specific antibody (BG4) prior
212 to adsorption of bacteria with G4-DNA/hemin on the surface, in order to block the contact
213 between G4-DNA/hemin and the electrode. We then monitored electron flow by
214 chronoamperometry. As a control, we coated the electrode with a non-specific anti-mouse
215 antibody. The non-specific antibody did not reduce electron flow (p value < 0.05), but the G4-
216 DNA-specific antibody reduced the current by approximately 1 nA (Fig. 2e). We therefore
217 conclude that G4-DNA/hemin must be in contact with the electrode to facilitate electron flow.
218
219 **G4-DNA/hemin incorporated into growing biofilms increases electron flow**
220 After measuring charge transfer and EET from adsorbed planktonic bacteria, we investigated
221 if G4-DNA and hemin could contribute to EET in biofilms where the G4-DNA integrate into a
222 larger eDNA network that facilitates electron transfer over longer distances. We inoculated
223 bacteria into media with G4-DNA, hemin or both, and grew biofilms directly on the electrode
224 surface (poised at 0.4 V) under anoxic conditions, prompting the bacteria to use the electrode
225 as electron acceptor. We measured the current produced throughout the 48 h of growth, and
226 subsequently visualized the biofilms by microscopy.
227 As expected, addition of G4-DNA did not promote a current from the biofilm to the electrode,
228 while addition of hemin did. The increase in current from hemin was, however, temporary and
229 started to decrease after 15 h. In contrast, the combination of G4-DNA and hemin resulted in a
230 stronger and more stable current throughout the 48 h incubation (Figure 3A). While the G4-
231 DNA in this experient were not generated naturally in the biofilm, our data is proof-of-concept
232 for the ability of G4-DNA structures to promote EET via hemin in biofilms.
233 Visualization of biofilms confirmed that G4-DNA was incorporated into the eDNA matrix
234 (Extended Data Fig. 6), and some G4-DNA formed nodule-like structures (Fig. 3b, Extended
235 Data Fig. 8). Similar DNA structures have been reported with electroactive *P. aeruginosa*
236 biofilms[1], but they did not investigate if the biofilms contained G4-DNA. G4-DNA can
237 aggregate through π-π interactions[12], and they can also cause liquid-liquid phase separation in

environments with molecular crowding[16]. It is not yet known how the nodule-like structures form and to which extent they contribute to electron transfer in the biofilm.

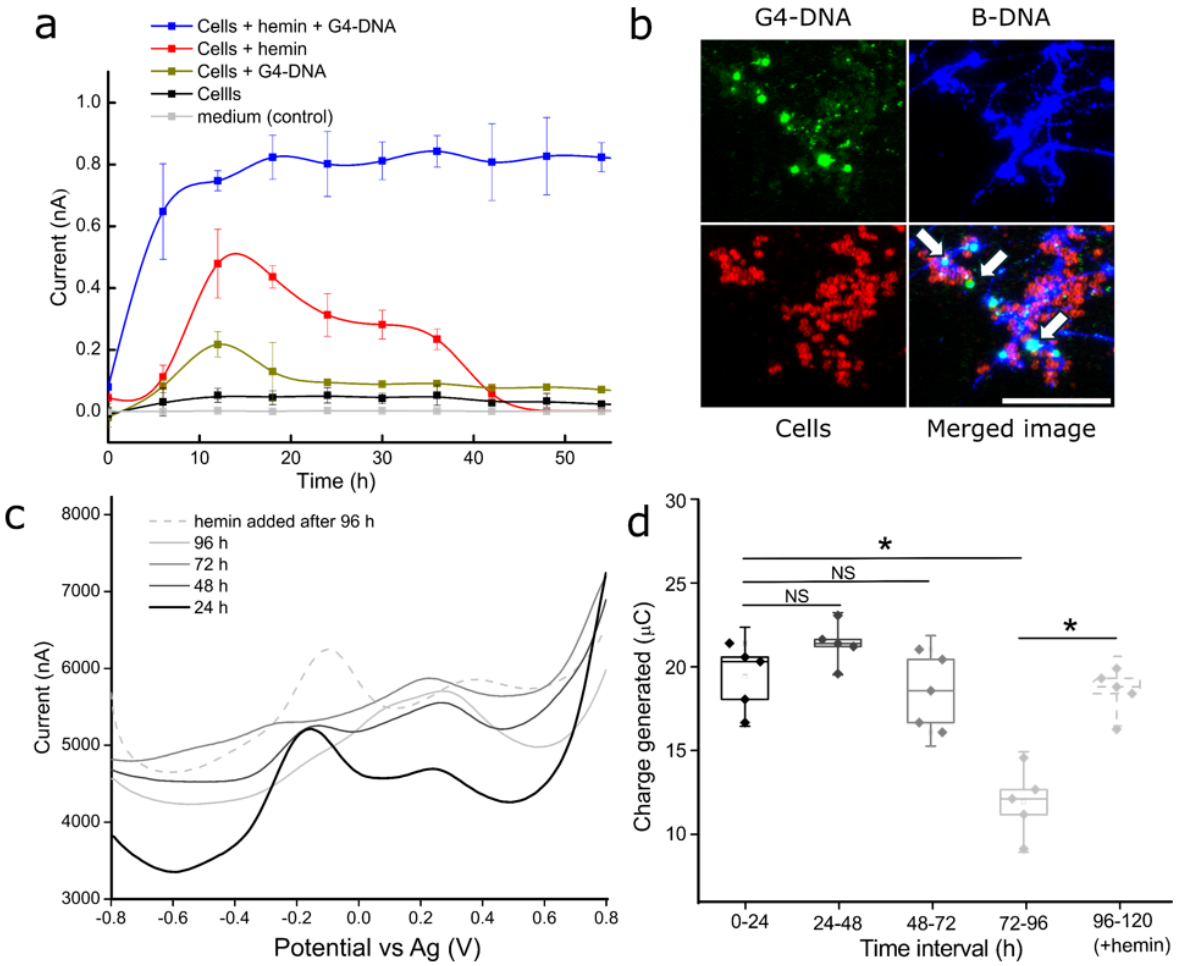

Fig. 3 Biofilms grown with G4-DNA and hemin exhibit electroactivity for up to 48 h and sustain electroactivity for longer with hemin replenishment.

a. Chronoamperometric measurements of *S. epidermidis* biofilm grown for 48 h on electrode surface poised at +0.4 V potential +/- addition of G4-DNA and hemin.

b. CLSM images of *S. epidermidis* biofilms formed on electrode surface after 48 h growth with G4-DNA and hemin. G4-DNA forms nodular structures (indicated by white arrows) that associate with B-DNA in the biofilm. Scalebar = 20 µm.

c. DPV of *S. epidermidis* biofilms grown with G4-DNA and hemin on electrode surface at +0.4 V potential. The current peak decreased after 24 h but could be recovered by replenishment of hemin.

d. Charge generated under different times tested from 0 h to 96 h, showing decrease in electroactivity close to the 96 h age of the biofilm in comparison with 120 h old biofilm treated with additional hemin immediately after 96th hour (∗ represents significant difference between labelled experimental conditions ($p < 0.05$) based on ANOVA and Tukey's test, NS: Not significant)

EET stability requires replenishment of hemin

Our initial results indicated that EET in biofilms was stronger and more stable over time when G4-DNA/hemin was incorporated into the biofilm matrix (Fig. 3a). To test the boundaries for how stable EET is over a longer time frame, we incubated biofilms for up to 96 h in a similar experiment and carried out DPV analyses on the biofilms every 24 h. The DPV peak at approx.. + 0.1-0.3 V ascribed to biomass increased from 0-48 h incubation and then remained stable, indicating that biofilms growth stagnated after 48 h incubation but subsequently stayed

265 associated with the electrode (Fig. 3c). Stagnation in biofilm growth was expected as the media
266 was not replenished at any time, and electron donors for metabolism would become depleted.
267 In accordance with the previous experiment, the peak around -0.1 to -0.3 V ascribed to G4-
268 DNA/hemin increased in height during the first 48 h, but subsequently decreased and
269 disappeared at 96 h incubation (Fig. 3c). The decrease in EET at 96 h was further corroborated
270 by measurement of charge transfer (Fig. 3d).
271 The decrease in EET could be caused by a decrease in metabolic activity as nutrients were
272 depleted from the media, or it could be caused by inactivation of the G4-DNA/hemin complex
273 due to e.g. oxidative damage or loss of Fe^{2+}. To test if it was the latter, we added 5 μM hemin
274 to the biofilm to replenish hemin in the G4-DNA structures. This resulted in restoration of the
275 G4-DNA/hemin DPV peak (Fig. 3c), indicating that EET activity of the G4-DNA/hemin
276 complex requires continuous replenishment of hemin to retain optimal activity over longer
277 timescales.
278
279 **Iron in hemin plays a key role in electroactivity of G4-DNA/hemin**
280 Hemin consists of protoporphyrin IX (PPIX) coordinating a ferric iron ion (heme B)[17]. To
281 validate the role of iron in EET observed in this study, we substituted hemin with the iron-
282 deficient PPIX and compared electrochemical signatures based on DPV and charge generated.
283 We grew biofilms on the electrode surface in media +/- G4-DNA and supplemented with either
284 PPIX or hemin for 48 h before DPV analysis. The DPV peak ascribed to free hemin (approx. -
285 0.35 V) was only observed in cell-free controls, indicating that free hemin had less interaction
286 with the biofilm-covered electrodes (Extended Data Fig. 7a). Biofilms grown with G4-DNA
287 and PPIX had only one prominent peak at approx. + 0.1-0.3 V, which we ascribed to biomass.
288 In contrast, biofilms grown with G4-DNA and hemin had two peaks: One ascribed to biomass
289 and one at -0.1 to -0.3 V ascribed to the hemin/G4-DNA complex, indicating that iron is
290 required for electroactivity. Furthermore, quantification of the charge generated from these
291 biofilms (Extended Data Fig. 7b) showed that electroactivity required the presence of iron in
292 hemin, and this result further corroborates iron's importance EET via G4-DNA/hemin.
293
294 **G4-DNA/hemin in the cell envelope facilitates electron transfer to hydrogen peroxide**
295 G4-DNA/hemin is a DNAzyme with peroxidase-like activity[18], and we therefore hypothesized
296 that it also facilitates transfer of electrons from bacteria to hydrogen peroxide, which then
297 becomes an electron acceptor for bacterial metabolism via EET.
298 We first confirmed the peroxidase activity of G4-DNA/hemin in *S. epidermidis* biofilms using
299 tyramide signal amplification (TSA). In this assay, the DNAzyme activates fluorescently
300 labeled tyramide in a reaction with H_2O_2, leading to immobilization of fluorescent tyramide to
301 near-by tyrosine. Biofilms amended with hemin showed a low level of extracellular peroxidase
302 activity – probably arising from G4-DNA/hemin complexes naturally present in the biofilm.
303 However, biofilms amended with both G4-DNA and hemin were strongly fluorescent,
304 confirming that the immobilized G4-DNA/hemin complex was catalytically active (Fig. 4a).
305 We then tested if the DNAzyme can transfer electrons from the bacteria's metabolism to H_2O_2
306 by characterising the electrochemical reduction of H_2O_2 in suspensions of *S. epidermidis* using
307 cyclic voltammetry (Fig. 4b). Addition of G4-DNA to the bacteria did not stimulate H_2O_2
308 reduction, while addition of hemin resulted in some H_2O_2 reduction (Extended Data Fig. 9).
309 However, the combination of G4-DNA and hemin resulted in highest reduction of H_2O_2 (Fig.
310 4b) apparent by the smaller CV oxidation and reduction curves (Fig. 4b). This trend was similar
311 to the electroactivity measured under the same conditions (Fig. 3a), indicating that G4-
312 DNA/hemin functioned as an electron conduit from the bacteria, transferring electrons from
313 bacteria to H_2O_2. Collectively the data shows that extracellular G4-DNA/hemin could expand

the repertoire of electron acceptors for *S. epidermidis,* and it might even protect the bacteria from H_2O_2 – one of the key components in how the immune system fights pathogens[19].

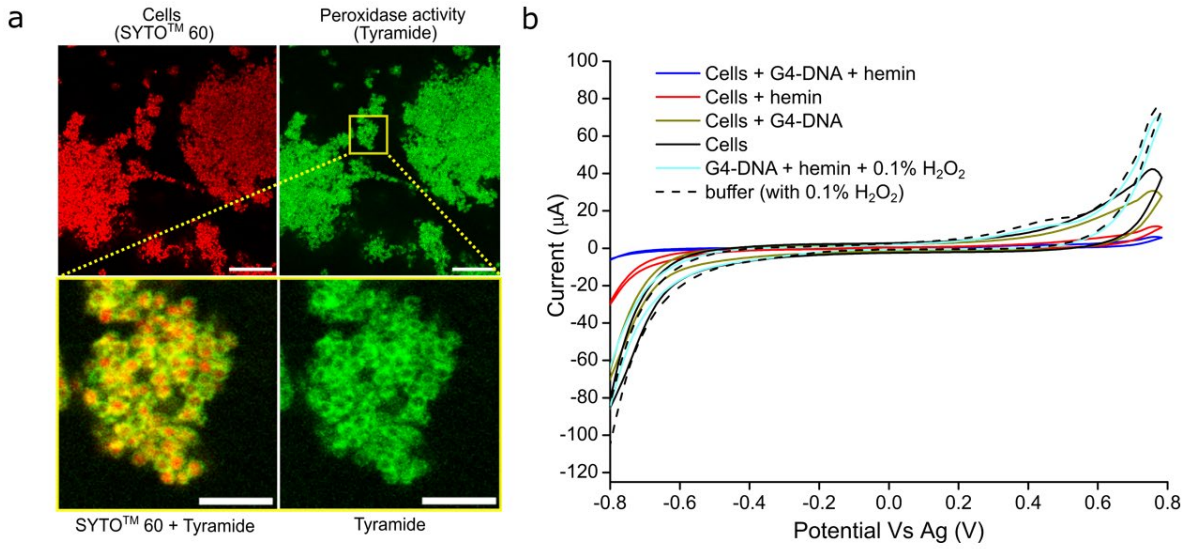

Fig. 4. G4-DNA/hemin is an extracellular DNAzyme with peroxidase-like activity that could electrocatalytically degrade hydrogen peroxide.
a. Tyramide signal amplification shows the location of extracellular peroxidase activity (green) in *S. epidermidis* (red, SYTO60™ stain) grown with xylose for PNAG inducation and subsequent amendment of G4-DNA and hemin. Scale bar = 20 µm. Zoomed image shows that the catalytic activity is associated with the bacterial surface. Scale bar = 5µm.
b. Electrocatalytic degradation of hydrogen peroxide with electrons from the bacteria. Cyclic voltammogram of electrochemical response from residual hydrogen peroxide in extracted peroxidase assay buffer after addition of cells, cells and hemin, cells and G4-DNA, or cells and G4-DNA/hemin complex.

DISCUSSION

This study is the first to present a role for non-canonical DNA structures in microbial EET. We first established that EET in *S. epidermidis* biofilms requires the presence of eDNA. Since this species is known to form an eDNA network that contains G4-DNA, we hypothesized that the hemin-binding properties of G4-DNA played a role in DNA-mediated EET. The lack of charge transfer from soluble hemin in the absence of G4-DNA underlines the importance of the G4-DNA/hemin complex for EET (Fig. 2 b,c). G4-DNA might increase charge transfer by hemin simply by facilitating its proximity to the cell, but charge transfer could also increase due to enhanced electroactivity of hemin in the G4-DNA/hemin complex[20,21] caused by the π-π stacking in G-quartets and the planar porphyrin structure of hemin[22]. Previous studies have shown that G4-DNA structures are an integral part of the eDNA network in staphylococcal biofilms[3], and we propose a mechanistic model for EET in biofilms where hemin-binding G4-DNA enables electron transfer to and from an "eDNA grid" that collectively leads to flow of electrons through the biofilm matrix (Fig. 5).
Electrons from metabolic processes enter the electron transport chain (ETC) of *S. epidermidis* when NADH and $FADH_2$ donate electrons to NADH dehydrogenase (NDH) or succinate dehydrogenase (SDH)[23]. NDH and SDH both transfer electrons to soluble menaquinone which transfers electrons to cytochromes and eventually to oxygen. In EET, electrons are diverted out of the cell. Based on the redox potential of hemin (-0.2 to -0.4 V vs Ag/AgCl), electrons are probably intercepted at NDH or SDH. NDH contributes to generating the proton motive force,

and diverting electrons from NDH to hemin in stead of menaquinol will still result in ATP production.

How might the electrons be transferred from NDH on the surface of the cell membrane to G4-DNA/hemin outside of the cell wall? G4-DNA structures are too wide to pass through the 2 nm pores of peptidoglycan, and the bacteria must use another mechanism to move electrons up through the peptidoglycan layer, which spans tens of nanometers. Electron flow across the cell envelope differs in Gram positive and Gram negative bacteria. While many electroactive Gram negative bacteria use multiheme cytochromes[24], these are uncommon in Gram positive bacteria such as *Staphylococcus*. In stead, Gram positive bacteria tend to secrete soluble redox mediators, such as nicotinaminde adenine dinucleotide (NAD) in *Bacillus subtilis*[25], and flavins and quinones in *Bacillus cereus*, *Rhodococcus ruber*[26] and *Lactiplantibacillus plantarum*[27]. *Listeria monocytogenes* immobilizes the secreted redox mediators in specific extracellular proteins (PplA) that span the peptidoglycan[28]. Another component that could facilitate electron transfer across the peptidoglycan are secreted conductive polymers. For example, *B. subtilis* forms long structures of poly γ-glutamic acid (γ-PGA) that make up a conductive biofilm matrix[9].

In our case, hemin may perform a similar role as secreted redox mediators, but rather than being secreted, pathogenic bacteria can aquire hemin from blood. At the site of an infection, hemin enters the blood as a result of hemolysis or tissue damage, reaching levels of up to 25 μM[29]. While hemin binds to G4-DNA with high specificity, it can also interact with other biomolecules and thereby become immobilised in the cell wall through such interactions. Hemin possesses a hydrophobic ring with a positively charged iron core, enabling interaction with proteins[30], lipids[31], and membrane vesicles[32]. Due to its positive charge and planar geometry, hemin might interact with lipo- or wall-teichoic acids, which are negatiely charged and constitute up to 50% of the cell wall mass[33]. It is thus possible that hemin contributes to electron transfer across the peptidoglycan, either as a soluble or immobilised redox mediator.

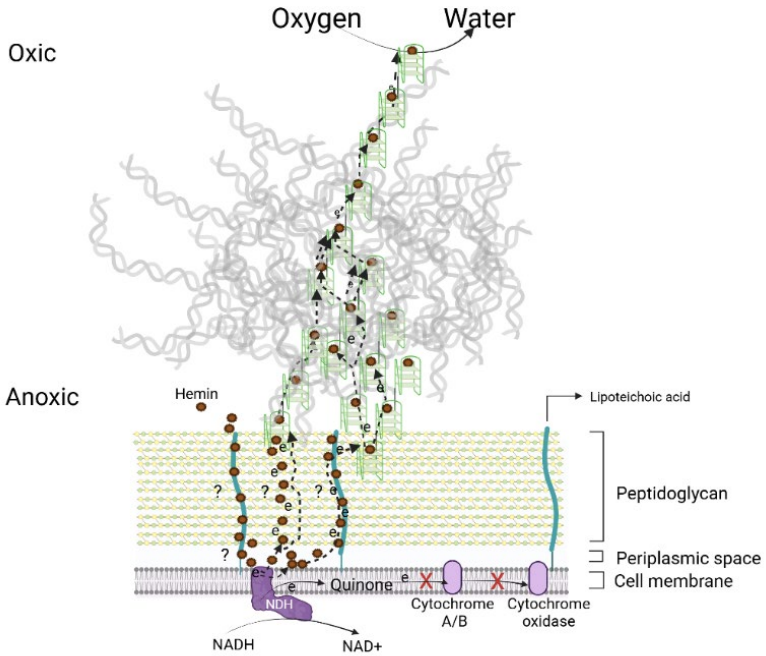

Fig. 5. A conceptual model for the proposed involvement of G4-DNA/hemin in eDNA-mediated EET in biofilms. Created in BioRender. Ajunwa, O. (2024) https://BioRender.com/h06f025

380
381 **Comparison with DNA-mediated EET in other bacteria**
382 DNA can be conductive in the right conformation and chemical environment. Canonical B-
383 DNA allows electrical charge transfer between π orbitals of closely arranged base pairs[34], and
384 DNA structures are being considered for programmable nanoelectronics[35] and batteries[36].
385 Notably, G4-DNA is more conductive than B-DNA because the stacked guanine tetrads
386 facilitate π-π interactions[37]. Multiple G4-DNA can also stack into conductive G-wires reaching
387 up to 100 nm[38]. This situates G4-DNA as a likely candidate for EET. DNA is the one matrix
388 component that most biofilms have in common and G4-DNA structures have so far been
389 reported in laboratory grown biofilms of *P. aeruginosa*[2] and *S. epidermidis,* in implant-
390 associated *S. aureus* infections[3], and in dental plaque[39]. It is thus likely that G4-DNA is present
391 in most biofilms, but its relevance was overlooked until now.
392 EET in biofilms can involve direct electron transfer via conductive biomolecules or indirect
393 electron transfer using soluble redox-active molecules[4,5,15] . Direct electron transfer via eDNA
394 has been shown in *Shewanella*[40], and a combination of direct and indirect electron transfer via
395 eDNA and phenazines was reported for *P. aeruginosa*[1]. With the vast abundance of iron
396 porphyrins in nature, we propose that G4-DNA and hemin provides a generic mechanism for
397 EET that is conceptually similar to what was described for *P. aeruginosa*.
398 We show in this study that *S. epidermidis,* which is not percieved as an electroactive
399 microorganism, does convey eDNA-dependent electron transfer in biofilms (Fig. 1). Moreover,
400 EET could be stimulated and maintained when providing additional G4-DNA and hemin to the
401 biofilms (Fig. 3a). We ascribe the stable EET to the immobilisation of hemin in the biofilm and
402 integration of electroactive G4-DNA/hemin complexes in the wider network of eDNA.
403 Furthermore, hemin in G4-DNA/hemin complexes may be better protected from oxidative
404 damage compared to free hemin [41], and thus provide a more stable EET.
405 The use of DNA for EET requires a mechanism by which electrons can be transferred to and
406 from the conductive DNA. While we propose that hemin is key to achieving such electron
407 transfer, there are also other DNA-binding redox-active molecules, such as flavins and
408 phenazines, which can increase DNA conductivity after being bound to DNA [1,42]. Similarly
409 chemosynthetic redox-active molecules such as methylene blue and monomethine
410 cyanine dyes have also been demonstrated to bind to G4-DNA [43,44]. The principle for eDNA-
411 mediated EET described in this study may therefore go far beyond the specific mechanism
412 described here.
413
414 **Biological implications of G4-DNA/hemin-mediated EET**
415 In nature, EET is usually associated with bacteria that use insoluble electron acceptors.
416 However, bacteria located in environments with steep chemical gradients can also use EET to
417 reach soluble electron donors at some distance from the cell[1]. This ability enables continued
418 respiration in anoxic microenvironments. In the infectious microenvironment, *S. epidermidis*
419 biofilms most likely experience such steep oxygen gradients, making a case for how EET
420 supports metabolic activity and survival of the population. The principle presented here is a
421 generic mechanism through which biofilm-producing bacteria can sustain respiration in anoxic
422 zones of a biofilm. As new research show that extracellular G4-DNA structures are common in
423 biofilms, we raise the question of whether EET might also be more widely used by
424 microorganisms than it was previously assumed.
425 Finally, we also show that H_2O_2 could be used as electron acceptor in EET due to the peroxidase
426 activity of the G4-DNA/hemin complex. *In vivo*, host cells produce H_2O_2 in response to the
427 infection[19], and bacteria in the infectious microenvironment might therefore use H_2O_2 as an
428 electron acceptor for respiration. In addition to facilitating respiration, the reaction may provide
429 an additional benefit by removing H_2O_2, which is part of the host defense system[45].

Another host defense mechanism is to limit the access of bacteria to iron[46]. Pathogens have therefore developed mechanisms to obtain iron from heme or hemin. For example, *S. aureus* contains near iron transporter (NEAT) domain proteins and Isd (iron-regulated surface determinant) for uptake of entire heme molecules from hemoproteins such as hemoglobin[47,48]. Furthermore, many staphylococci produce staphyloferrin siderophores that bind and assist the uptake of free iron. *S. epidermidis* lacks the machinery for heme uptake, but utilises sideophores such as staphyloferrin A[49]. Immobilisation of hemin on the cell envelope may serve as a mechanism for accessing iron in the infectious microenvrionment, and this phenomenon could explain the increase in growth yield caused by hemin when bacteria contained surface-associated G4-DNA (Extended Data Fig. 3).

Acknowledgments

This work was funded by the Danish council for independent research, grant no. 2032-00294B. The authors thank Professors Lars Peter Nielsen and Andreas Schramm and the Center for Electromicrobiology (CEM) Aarhus University, Denmark for insightful discussions during the project. The authors also thank Professor Dr. Holger Rohde of Universitätsklinikum Hamburg-Eppendorf, Germany, for providing us with the *Staphylococcus epidermidis* strains used in this work. Graduate student Elena Bouvier is also appreciated for assistance in preliminary laboratory work during her internship at the Interdisciplinary Nanoscience Center, Aarhus University, Denmark.

Author contributions

OMA: Investigation, methodology, data curation, data analyses, writing – original draft, writing – review and editing

GASM: Methodology, writing – review and editing

SDJ: Investigation, data curation, writing – review and editing,

RLM: Fund acquisition, methodology, data curation, writing – original draft, writing – review and editing

References

1 Saunders, S. H. *et al.* Extracellular DNA Promotes Efficient Extracellular Electron Transfer by Pyocyanin in Pseudomonas aeruginosa Biofilms. *Cell* **182**, 919-932.e919, doi:10.1016/j.cell.2020.07.006 (2020).

2 Seviour, T. *et al.* The biofilm matrix scaffold of Ps eudomonas aeruginosa contains G-quadruplex extracellular DNA structures. *npj Biofilms and Microbiomes* **7**, doi:10.1038/s41522-021-00197-5 (2021).

3 Minero, G. Antonio S. *et al.* Extracellular G-quadruplexes and Z-DNA protect biofilms from DNase I, and G-quadruplexes form a DNAzyme with peroxidase activity. *Nucleic Acids Research* **52**, 1575-1590, doi:10.1093/nar/gkae034 (2024).

4 Gorby, Y. A. *et al.* Electrically conductive bacterial nanowires produced by Shewanella oneidensis strain MR-1 and other microorganisms. *Proceedings of the National Academy of Sciences* **103**, 11358-11363, doi:doi:10.1073/pnas.0604517103 (2006).

5 Rotaru, A.-E. *et al.* Direct Interspecies Electron Transfer between Geobacter metallireducens and Methanosarcina barkeri. *Applied and Environmental Microbiology* **80**, 4599-4605, doi:doi:10.1128/AEM.00895-14 (2014).

6 Sydow, A., Krieg, T., Mayer, F., Schrader, J. & Holtmann, D. Electroactive bacteria—molecular mechanisms and genetic tools. *Applied Microbiology and Biotechnology* **98**, 8481-8495, doi:10.1007/s00253-014-6005-z (2014).

7 Digel, L., Bonné, R. & Aiyer, K. Are all microbes electroactive? *Cell Reports Physical Science* **5**, doi:10.1016/j.xcrp.2024.102200 (2024).

8 Zhuang, Z. *et al.* Physiological potential of extracellular polysaccharide in promoting Geobacter biofilm formation and extracellular electron transfer. *Science of the Total Environment* **741**, doi:10.1016/j.scitotenv.2020.140365 (2020).

9 Adilkhanova, A. *et al.* Electrofermentation increases concentration of poly γ-glutamic acid in Bacillus subtilis biofilms. *Microbial Biotechnology* **17**, doi:10.1111/1751-7915.14426 (2024).

10 Buzzo, J. R. *et al.* Z-form extracellular DNA is a structural component of the bacterial biofilm matrix. *Cell* **184**, 5740-5758.e5717, doi:10.1016/j.cell.2021.10.010 (2021).

11 Mugunthan, S. *et al.* RNA is a key component of extracellular DNA networks in Pseudomonas aeruginosa biofilms. *Nature Communications* **14**, 7772, doi:10.1038/s41467-023-43533-3 (2023).

12 Li, J. *et al.* Zippered G-quadruplex/hemin DNAzyme: exceptional catalyst for universal bioanalytical applications. *Nucleic Acids Research* **49**, 13031-13044, doi:10.1093/nar/gkab1178 (2021).

13 Christner, M. *et al.* The giant extracellular matrix-binding protein of Staphylococcus epidermidis mediates biofilm accumulation and attachment to fibronectin. *Mol Microbiol* **75**, 187-207, doi:10.1111/j.1365-2958.2009.06981.x (2010).

14 Yang, X. *et al.* Stress-assisted microbiologically influenced corrosion mechanism of 2205 duplex stainless steel caused by sulfate-reducing bacteria. *Corrosion Science* **173**, 108746, doi:https://doi.org/10.1016/j.corsci.2020.108746 (2020).

15 Huang, H. *et al.* Bidirectional extracellular electron transfers by Stenotrophomonas sp. and by Serratia marcescens via tunable extracellular polymeric substances at low or at high solution conductivity. *Electrochimica Acta* **506**, 145048, doi:https://doi.org/10.1016/j.electacta.2024.145048 (2024).

16 Amin, A. & Oyoshi, T. in *Phase Separation in Living Cells: Benefits and Risks* (ed Riki Kurokawa) 39-57 (Springer Nature Singapore, 2023).

17 Cvjetan, N. & Walde, P. Ferric heme b in aqueous micellar and vesicular systems: state-of-the-art and challenges. *Quarterly Reviews of Biophysics* **56**, e1, doi:10.1017/S0033583522000130 (2023).

18 Ghahremani Nasab, M., Hassani, L., Mohammadi Nejad, S. & Norouzi, D. Interaction of hemin with quadruplex DNA. *J Biol Phys* **43**, 5-14, doi:10.1007/s10867-016-9430-7 (2017).

19 Wittmann, C. *et al.* Hydrogen peroxide in inflammation: messenger, guide, and assassin. *Adv Hematol* **2012**, 541471, doi:10.1155/2012/541471 (2012).

20 Tianjun, C. *et al.* Activity Enhancement of G-quadruplex/hemin DNAzyme by Flanking d(CCC). *Chemistry - A European Journal* **22**, doi:10.1002/chem.201504797 (2016).

21 Bi, Q., Qiu, F., Yuan, R. & Xiang, Y. In situ formation of G-quadruplex/hemin nanowires for sensitive and label-free electrochemical sensing of acid phosphatase. *Sensors and Actuators B: Chemical* **330**, 129272, doi:https://doi.org/10.1016/j.snb.2020.129272 (2021).

22 Wang, Z. & Liu, J.-P. Effects of the central potassium ions on the G-quadruplex and stabilizer binding. *Journal of Molecular Graphics and Modelling* **72**, 168-177, doi:https://doi.org/10.1016/j.jmgm.2017.01.006 (2017).

23 Uribe-Alvarez, C. *et al.* Staphylococcus epidermidis: metabolic adaptation and biofilm formation in response to different oxygen concentrations. *Pathogens and Disease* **74**, doi:10.1093/femspd/ftv111 (2015).

24 Breuer, M., Rosso, K. M. & Blumberger, J. Electron flow in multiheme bacterial cytochromes is a balancing act between heme electronic interaction and redox potentials. *Proceedings of the National Academy of Sciences* **111**, 611-616, doi:doi:10.1073/pnas.1316156111 (2014).

25 Chen, L. *et al.* Electron Communication of Bacillus subtilis in Harsh Environments. *iScience* **12**, 260-269, doi:10.1016/j.isci.2019.01.020 (2019).

26 Tian, T. *et al.* Flavin-mediated extracellular electron transfer in Gram-positive bacteria Bacillus cereus DIF1 and Rhodococcus ruber DIF2. *RSC Adv* **9**, 40903-40909, doi:10.1039/c9ra08045g (2019).

27 Tolar, J. G., Li, S. & Ajo-Franklin, C. M. The Differing Roles of Flavins and Quinones in Extracellular Electron Transfer in Lactiplantibacillus plantarum. *Applied and Environmental Microbiology* **89**, e01313-01322, doi:doi:10.1128/aem.01313-22 (2023).

28 Light, S. H. *et al.* A flavin-based extracellular electron transfer mechanism in diverse Gram-positive bacteria. *Nature* **562**, 140-144, doi:10.1038/s41586-018-0498-z (2018).

29 Schaer, D. J., Buehler, P. W., Alayash, A. I., Belcher, J. D. & Vercellotti, G. M. Hemolysis and free hemoglobin revisited: exploring hemoglobin and hemin scavengers as a novel class of therapeutic proteins. *Blood* **121**, 1276-1284, doi:10.1182/blood-2012-11-451229 (2013).

30 Brewitz, H. H., Hagelueken, G. & Imhof, D. Structural and functional diversity of transient heme binding to bacterial proteins. *Biochimica et Biophysica Acta (BBA) - General Subjects* **1861**, 683-697, doi:https://doi.org/10.1016/j.bbagen.2016.12.021 (2017).

31 Bonamore, A. *et al.* Interaction with membrane lipids and heme ligand binding properties of Escherichia coli flavohemoglobin. *Biochemistry* **42**, 5792-5801, doi:10.1021/bi0206311 (2003).

32 Wang, M., Nie, Y. & Wu, X.-L. Extracellular heme recycling and sharing across species by novel mycomembrane vesicles of a Gram-positive bacterium. *The ISME Journal* **15**, 605-617, doi:10.1038/s41396-020-00800-1 (2021).

33 Caudill, E. R. *et al.* Wall teichoic acids govern cationic gold nanoparticle interaction with Gram-positive bacterial cell walls. *Chemical Science* **11**, 4106-4118, doi:10.1039/C9SC05436G (2020).

34 Endres, R. G., Cox, D. L. & Singh, R. R. P. Colloquium: The quest for high-conductance DNA. *Reviews of Modern Physics* **76**, 195-214, doi:10.1103/RevModPhys.76.195 (2004).

35 Jeong, H. *et al.* Electronic Activation of a DNA Nanodevice Using a Multilayer Nanofilm. *Small* **12**, 5572-5578, doi:https://doi.org/10.1002/smll.201601273 (2016).

36 Ouyang, Z. *et al.* Programmable DNA Interphase Layers for High-Performance Anode-Free Lithium Metal Batteries. *Advanced Materials* **36**, 2401114, doi:https://doi.org/10.1002/adma.202401114 (2024).

37 Zhang, L., Zhang, J. & Ulstrup, J. Electrochemical single-molecule conductivity of duplex and quadruplex DNA. *Current Opinion in Electrochemistry* **4**, 166-174, doi:https://doi.org/10.1016/j.coelec.2017.11.009 (2017).

38 Pavc, D. *et al.* Understanding self-assembly at molecular level enables controlled design of DNA G-wires of different properties. *Nature Communications* **13**, 1062, doi:10.1038/s41467-022-28726-6 (2022).
39 Evans, D. C. S. *et al.* Dental biofilms contain DNase I-resistant Z-DNA and G-quadruplexes. *bioRxiv*, 2024.2010.2013.618059, doi:10.1101/2024.10.13.618059 (2024).
40 Furst, A. L., Smith, M. J., Lee, M. C. & Francis, M. B. DNA Hybridization To Interface Current-Producing Cells with Electrode Surfaces. *ACS Cent Sci* **4**, 880-884, doi:10.1021/acscentsci.8b00255 (2018).
41 Zhang, M. *et al.* Cell-free hemoglobin and hemin catalyzing triclosan oxidative coupling in plasma: A novel exogenous phenolic pollutants coupling pathway. *Ecotoxicology and Environmental Safety* **282**, 116708, doi:https://doi.org/10.1016/j.ecoenv.2024.116708 (2024).
42 Merkle, T., Sinn, M. & Hartig, J. S. Interactions between Flavins and Quadruplex Nucleic Acids. *Chembiochem* **16**, 2437-2440, doi:10.1002/cbic.201500463 (2015).
43 Kékedy-Nagy, L., Kotlyar, A. B. & Ferapontova, E. E. Long-range electron transfer mediated by G-quadruplex wires attached to gold electrodes via phosphorothioated dA tags. *Electrochimica Acta* **476**, 143761, doi:https://doi.org/10.1016/j.electacta.2024.143761 (2024).
44 Fabijanić, I. *et al.* Selenium-Substituted Monomethine Cyanine Dyes as Selective G-Quadruplex Spectroscopic Probes with Theranostic Potential. *Biomolecules* **13**, doi:10.3390/biom13010128 (2023).
45 Kato, Y. Neutrophil myeloperoxidase and its substrates: formation of specific markers and reactive compounds during inflammation. *J Clin Biochem Nutr* **58**, 99-104, doi:10.3164/jcbn.15-104 (2016).
46 Ullah, I. & Lang, M. Key players in the regulation of iron homeostasis at the host-pathogen interface. *Front Immunol* **14**, 1279826, doi:10.3389/fimmu.2023.1279826 (2023).
47 Alfeo, M. J. *et al.* Staphylococcus aureus iron-regulated surface determinant B (IsdB) protein interacts with von Willebrand factor and promotes adherence to endothelial cells. *Scientific Reports* **11**, 22799, doi:10.1038/s41598-021-02065-w (2021).
48 Zapotoczna, M., Heilbronner, S., Speziale, P. & Foster, T. J. Iron-regulated surface determinant (Isd) proteins of Staphylococcus lugdunensis. *J Bacteriol* **194**, 6453-6467, doi:10.1128/jb.01195-12 (2012).
49 Oliveira, F., Rohde, H., Vilanova, M. & Cerca, N. Fighting Staphylococcus epidermidis Biofilm-Associated Infections: Can Iron Be the Key to Success? *Frontiers in Cellular and Infection Microbiology* **11**, doi:10.3389/fcimb.2021.798563 (2021).
50 Rohde, H. *et al.* Induction of Staphylococcus epidermidis biofilm formation via proteolytic processing of the accumulation-associated protein by staphylococcal and host proteases. *Mol Microbiol* **55**, 1883-1895, doi:10.1111/j.1365-2958.2005.04515.x (2005).
51 Galac, M. R. *et al.* Complete Genome Sequence of Staphylococcus epidermidis 1457. *Genome Announc* **5**, doi:10.1128/genomeA.00450-17 (2017).
52 Skovdal, S. M. *et al.* Host factors abolish the need for polysaccharides and extracellular matrix-binding protein in Staphylococcus epidermidis biofilm formation. *J Med Microbiol* **70**, doi:10.1099/jmm.0.001287 (2021).
53 Han, E. J. Y., Palanisamy, K., Hinks, J. & Wuertz, S. Parameter Selection for a Microvolume Electrochemical Escherichia coli Detector for Pairing with a Concentration Device. *Sensors (Basel)* **19**, doi:10.3390/s19112437 (2019).

607 **METHODS**
608
609 **Chemicals and fluorescent stains**
610 All chemicals used were first made as stock solutions. Hemin (Merck®) and protoporphyrin
611 IX (Merck®) were prepared as 10 mM stock solutions in 200 mM Tris, 30 % DMSO and 100
612 mM NaOH (Merck®) at pH 11, and protected from light. Tris (Tris hydroxymethyl amino
613 methane, pH 7.5, Merck®), modified MES buffer (25 mM MES (Sigma, M3671), 0.2 M NaCl
614 (Sigma, S5886), and 0.010 M KCl (Sigma, 1.04936)) and DMSO stocks were prepared with
615 filter-sterilized deionized water. Salts and sugars; NaCl, KCl and xylose were prepared as
616 sterile filtered 1M stocks for buffer and culture preparations. Acetic acid (30% v/v) was used
617 for pH adjustment of Tris buffers when prepared. Annealing buffer for G4-DNA was prepared
618 by mixing 10 mM Tris, with 100 mM KCl (pH 7.2) and adjusting to pH 6.5 with acetic acid.
619 Tyramide reagent was prepared by adding tyramide conjugated with Alexa Fluor 488 (1:100)
620 (Invitrogen, B40953), 2 mM ATP (Thermo Scientific, R0441), and 0.1% hydrogen peroxide
621 (Sigma, 216763) in modified MES buffer.
622 DNA binding stain SYTO^{TM} 60 (20 µM working concentration), was prepared as 100 x aliquots
623 in sterile deionized water before use. A lipophilic dye FM 4-64 was prepared by mixing with
624 sterile distilled water to 1mg/mL stock concentration. Working concentration for FM-464 was
625 10 µg/mL and aliquots for stains were made before storage at -20ºC.
626
627 **Synthetic DNA, annealing and characterisation conditions**
628 Oligonucleotides of guanine quadruplex (G4-DNA) sequences were purchased from Integrated
629 DNA technologies (IDT), Belgium, as 100 µM stock in 1 mM Tris EDTA buffer. We used a
630 monomer and a trimer of the c-Myc oncogene known to form G-quadruplex structures: c-
631 Myc1: 5´- GA**GGGTGGGTAGGGTGGG**CGTCAACAGACTCGA-3´) and c-Myc3: 5´-
632 GA**GGGTGGGTAGGGTGGGGAGGGTGGGTAGGGTGGGGAGGGTGGGTAGGG**
633 **TGG**GCGTCAACAGACTCGA -3´. The part of the sequence that forms G-quadruplex is
634 highlighted in bold. DNA annealing of oligonucleotides was done in an annealing buffer with
635 composition stated above. Annealing was done by preparing 100 µL of 50 µM oligonucleotide
636 stock in annealing buffer (pH 6.5), heating to 90ºC for 3 min, and gradual cooling to 30ºC. The
637 structure of annealed oligonucleotides was confirmed by recording the circular dichroism (CD)
638 spectrum using a J-810 spectropolarimeter at 220 – 320 nm, scanning speed 50 nm/min, and 2
639 nm bandwidth, and ultraviolet/visible spectrophotometer (UV/vis) also at 220 – 320 nm. For
640 CD and UV/vis measurements, 5 µM oligonucleotides were prepared from sub-stocks and 70
641 µL sample was loaded into the spectropolarimeter and spectrophotometer respectively. CD
642 signals were converted to ellipticity $\Delta\varepsilon$ (M^{-1} cm^{-1}) using Beer-Lambert's law and recorded.

643
644 **Strains, cultures and media**
645 Tryptic soy broth medium (TSB, Merck) and Brain heart infusion medium (BHI, Merck) were
646 prepared according to manufacturers' specifications and used for culture preparations. Solid
647 agar plates were prepared by mixing broth medium with 15 g/L agar powder. Autoclaved media
648 broths supplemented with additional 200 mM NaCl were used for growing bacteria in overnight
649 cultures. Bacterial cultures were made as overnight cultures by inoculating from single colonies
650 on agar into 20 mL BHI/NaCl or TSB/NaCl broth depending on culture requirement and
651 incubated for 15 – 20 h at 37ºC with constant agitation at 150 rpm. *S. epidermidis* 1457, *S.*
652 *epidermidis* 1457 Δ*atlE*, *S. epidermidis* 1585 pTX*icaADBC* were used in this study [13,50-52].
653 Strains were stored at -80ºC as stock cultures in cryotubes in 30% glycerol. For experiments
654 with hemin, TSB/NaCl medium was supplemented with 5 µM hemin unless stated otherwise.

655
656 **Visualization of G4-DNA structures by immunolabeling**
657 Fluorescence-conjugated antibodies were used for immunolabeling of DNA structures. G4-
658 DNA specific antibody BG4 (goat monoclonal IgG lambda, Ab00174-24.1) with 0.02 %
659 proclin was purchased as 1 mg/mL preparations in phosphate buffered saline (PBS) from
660 Absolute Antibodies® with the fluorescent label Atto 488 and stored at 4ºC. B-DNA specific
661 antibody AB1.227156 (mouse monoclonal, AB27156, 1068371-2) was purchased from
662 Abcam® without a fluorescent label. An anti-mouse antibody (goat monoclonal IgG H + L,
663 XF346503 Invitrogen®) labelled with AlexaFluo405 was purchased as 2 mg/mL preparation
664 in PBS with 0.05 % sodium azide and 50% glycerol and stored at -20ºC and used as a secondary
665 antibody for B-DNA detection (AB2). Both antibodies were mixed with 3 % bovine serum
666 albumin (BSA) in PBS, which served as a blocking agent for non-specific binding during
667 immunolabeling experiments.
668 Planktonic cultures were suspended for 2 min in 3% BSA in PBS before addition of BG4
669 antibody (working concentration 1:100 in 3 % BSA in PBS) and incubation for 90 min at room
670 temperature. Immunolabeled bacteria were then briefly washed in 100 mM KCl and transferred
671 to glass slides for microscopy.
672 For biofilm samples, the medium was removed and biofilms were gently washed with 3 % BSA
673 in PBS before adding 60 µL BG4 antibody (1: 100) in 3% BSA in PBS and incubating for 90
674 min with gentle shaking at 50 rpm at room temperature. Without washing or decanting, 60 µL
675 AB1 (1:100) in 3 % BSA was added and samples were incubated for another 90 min under the
676 same conditions. For the next step, biofilms were gently washed with 3% BSA before the
677 addition of 60 µL of the secondary antibody AB2 (1: 100) in 3 % BSA in PBS and 60 min
678 incubation. Finally, biofilms were washed with 3% BSA in PBS and stained with 10 µg/mL
679 FM-464 solution in 100 mM NaCl to visualize the bacteria.
680 Confocal laser scanning microscopy was performed using a LSM700 microscope (Carl Zeiss)
681 equipped with a 63x objective (Plan-Apochromat, NA1.4 oil immersion objective). We used
682 the bright field transmission to see unstained bacteria, 488 nm excitation and >660 nm emission
683 to visualize FM4-64 stained bacteria, 488 nm excitation and 520 – 600 nm emission for the
684 Atto-488 conjugated BG4 antibody, and 405 excitation and 410-477 nm emission for the
685 AlexaFlour 405-conjugated AB2 antibody.
686
687 **Establishment of an experimental model with high or low amounts of G4-DNA**
688 To investigate the contribution of G4-DNA to EET, we first established an experimental model
689 in which bacteria contained many or few G4/hemin complexes associated with the bacterial
690 surface. We hypothesized that G4-DNA would associate with extracellular polysaccharides and
691 therefore acquired a strain in which polysaccharide production could be controlled via an
692 inducible promoter. *S. epidermidis* 1585 pTX*icaADBC* was grown overnight in BHI/NaCl
693 supplemented with tetracycline (20 µg/ml), and xylose (2% w/v) to induce production of poly-
694 n-acetyl glucosamine (PNAG). Bacteria grown in the absence of xylose were used as a
695 polysaccharide-deficient control.
696 To prepare the experimental model, overnight culture of bacteria were collected in 1 mL broth
697 and centrifuged (5 min at 906 × *g*), washed, and resuspended in 100 mM KCl to an optical
698 density at 600 nm (OD_{600}) of 0.5. Annealed G4-DNA (5 µM) and/or hemin (5 µM) was added
699 (5 µM hemin best supported hemin tolerance by *S. epidermidis*), and samples were vortexed
700 (1 min), incubated at room temperature for 1 h in the dark, centrifuged (2 min at 906 × *g*), and
701 resuspended in 100 mM KCl to wash away unbound G4-DNA or hemin. Surface-bound G4-
702 DNA was visualized by fluorescence immunolabeling as described above.
703 Annealed c-Myc1 and c-Myc3 G4-DNA sequences were adsorbed on PNAG producing *S.*
704 *epidermidis* 1585 pTX*icaADBC* separately and immunolabelled for comparison. After

705 confirming that *S. epidermidis* 1585 pTX*icaADBC* could adsorb G4-DNA to the bacterial
706 surface when PNAG production was induced, this strain was used as a model organism with
707 high or low amount of G4-DNA structures in the subsequent experiments. All subsequent
708 experiments were done with the G4-DNA sequence with highest binding.
709 Prior to the experimental model, concentrations of G4-DNA/hemin concentration tolerable to
710 planktonic cells were determined and used for subsequent experiments with the *S. epidermidis*
711 1585 pTX*icaADBC* strain. BHI/NaCl broths supplemented with tetracycline (20 µg/ml), with
712 and without xylose (2 % w/v) were prepared to test the effect of PNAG production by
713 planktonic cells on hemin tolerance. Overnight cultures were collected in 1 mL broths,
714 centrifuged (5 min at 906 × *g*) and pellets were resuspended in same medium broths to an
715 optical density (OD_{600}) of 0.01 in 2 mL volumes before transferring to sterile 48 well plates
716 (Sarstedt AG & Co). Different hemin concentrations (0, 5, 40 and 200 µM) +/- 5 µM, annealed
717 c-Myc3 were then added. Unlike hemin, G4-DNA was not considered toxic, and concentration
718 used (5 µM) in this experiment was kept constant. Experiments were carried out in triplicates
719 and kept in the dark. Microtitre plates with culture were incubated for 24 h with shaking (100
720 rpm) at 37 ºC. After incubation, 0.1 mL of each of the cultures were serially diluted 10-fold in
721 sterile deionized water. Dilution 10^{-7} was plated onto BHI agar by transferring 0.1 mL on the
722 agar. Inoculum were evenly spread on the agar using sterile cell spreader. Agar plates were
723 incubated at 37 ºC for 24 h. Colonies were counted after incubation and CFU/mL was
724 determined. Logarithmic values of the CFU/mL were calculated and recorded.
725
726 **Electroanalysis of planktonic bacteria adsorbed to the electrode**
727 *S. epidermidis* 1585 pTX*icaADBC* was grown overnight in BHI/NaCl supplemented with
728 tetracycline (20 µg/ml), and +/- xylose (2% w/v) to induce polysaccharide production. Bacteria
729 were washed by centrifugation (5 min at 1118 × *g*) and adjusted to OD_{600} 0.5 in 100 mM KCl
730 with G4-DNA and/or hemin treatments as described above. For comparison, electroanalyses
731 with planktonic *S. epidermidis* 1457 and *S. epidermidis* 1457 Δ*atlE* were also carried out on
732 overnight cultures grown in BHI/NaCl, washed and suspended in 100 mM KCl to OD_{600} 0.5
733 with G4-DNA + hemin treatment as described above.
734 The SPEs (Metrohm DropSens DRP-C110, Metrohm Spain) had a 4 mm diameter transparent
735 Indium Tin Oxide (ITO) working electrode (WE) with surface area of 0.126 cm^2, a graphite
736 counter electrode, and Ag pseudo-reference electrode. Prior to use, SPEs were sterilized in 70%
737 v/v ethanol, washed thrice in sterile deionized water, and air dried. Bacterial suspensions (100
738 µL) were then deposited on screen printed electrodes (SPEs) and left to adsorb for 15 min.
739 During deposition, cells were made to cover the whole surface area of working, reference and
740 counter electrode. Excess cells were gently rinsed with 100 mM KCl and SPEs were
741 subsequently connected to a computer-controlled multichannel PalmSens 4 potentiostat
742 (PalmSens® Netherlands) equipped with an EmStatMUX8-R2 multiplexer.
743 All electrochemistry data were collected and analysed using the PalmSens PsTrace 5.9
744 software. Cyclic voltammetry (CV) was run between -0.8V and 0.8V with a step size of 0.01
745 V and a scan rate of 0.05 V/s for 3 scan cycles, and the last scan was selected per sample.
746 Samples were run in triplicates and the averages were plotted. Differential pulse voltammetry
747 (DPV) was carried out by first pretreating at 0.2 V for 2 min before running with -0.8 V as start
748 potential and 0.8 V as end potential, with scan rate of 0.05 V/s, step size 0.01 V, pulse time 0.02
749 s and current range from 10 nA to 1mA. The average scans of three biological replicates were
750 recorded for each voltammetric experiment.
751 Chronoamperometry (CA) was also carried out using 0.4 V poised potentials for 300 s after
752 200 s pre-treatment and delay time to allow the bacteria to acclimatize to the poised potential.
753 Values of total charge generated were also recorded after the CA measurements. Multi-step

754 chronamperometry (MSCA) was carried out by switching between poised potentials 0.4 V and
755 -0.4V for 30 s with 3 s between switches.
756 At the end of the experiment, the adsorbed bacteria and the presence of G4-DNA structures
757 were visualized by immunolabeling and microscopy as described above. Comparative CV
758 analyses was carried out on c-Myc1 and c-Myc3 G4DNA treated planktonic cells of
759 polysaccharide producing *S. epidermidis* 1585 pTX*icaADBC* in the presence of hemin. G4-
760 DNA with higher electroactivity was selected for further analyses.
761
762 **Blocking of electron transfer with G4-DNA-binding antibodies**
763 We sought to validate the contribution of G4-DNA/hemin to electroactivity, as hemin could
764 potentially also associate with other biomolecules on the bacterial surface. We therefore used
765 a G4-DNA specific antibody to block the electron flow from G4-DNA/hemin on bacteria to the
766 electrode. Overnight cultures of *S. epidermidis* 1585 pTX*icaADBC* were prepared, suspended
767 in 100 mM KCl, treated with G4-DNA and hemin, and deposited on SPEs as described above.
768 However, before depositing bacteria, SPEs were treated with 60 µL BG4 antibody (1: 100 in
769 3% BSA in PBS) or a non-specific antibody (anti-mouse antibody - goat monoclonal IgG H +
770 L, XF346503 Invitrogen®), and allowed to dry for 30 min. As controls SPEs were treated with
771 BG4 antibody alone or G4-DNA (5 µM). CA was carried out using 0.4 V poised potentials as
772 described above.
773
774 **Electroanalysis of *S. epidermidis* biofilms grown directly on screen printed electrodes**
775 We first aimed to use a wildtype *S. epidermidis* (strain 1457) and an eDNA-negative mutant
776 (*S. epidermidis* 1457 Δ*atlE*) to determine if *S. epidermidis* biofilms are electroactive, and if this
777 activity correlates with the presence of eDNA. We used *S. epidermidis* 1457 for this purpose
778 because previous publications had documented formation of G4-DNA in the biofilm eDNA
779 network formed by this strain.
780 Overnight cultures grown in TSB/NaCl were centrifuged (2 min at 5000 rpm) and transferred
781 to TSB/NaCl with 5 µM hemin, adjusted to OD_{600} of 0.05, and 1.5 mL was then transferred to
782 sterile 2 mL polystyrene cuvettes (Sarstedt AG & Co). Sterile SPEs were inserted into the
783 solution (the connective end of SPEs was not submerged) and incubated at 150 rpm for 48 h
784 before analysis by CV and DPV to determine the electrochemical peaks as described above.
785 The average scans of three biological replicates were recorded for each voltammetric
786 experiment. As a control experiment to separate the activity of biofilms from planktonic
787 bacteria, planktonic cultures of both strains were grown for 48 h in TSB/NaCl + 5 µM hemin,
788 and sterile SPEs were inserted into the culture for DPV analyses of the planktonic culture.
789 *S. epidermidis* 1457 may not naturally produce a large and controllable amount of G4-DNA
790 structures in the biofilm. To better understand how G4-DNA can contribute to EET in biofilms,
791 we therefore used our experimental model *S. epidermidis* 1585 +/- PNAG production and +/-
792 addidion of G4-DNA oligos to study EET in biofilms with high or low amounts of G4-DNA
793 structures in the extracellular matrix.
794 *S. epidermidis* 1585 pTX*icaADBC* biofilms were grown in 1 mL anaerobic custom-made
795 containers mounted directly on the SPEs. A 10 mm diameter glass vial with butyl rubber cap
796 was cut to remove the glass bottom. The top was then attached to the SPE using non-conductive
797 glue as described in Han et al. [53] with slight modifications. The container was sterilised with
798 70% ethanol and UV light for 15 min. BHI/NaCl (0.5 mL) with 2% xylose and/or hemin (5
799 µM) and G4-DNA (5 µM) was added and sparged with N_2 gas for 2 min using sterile needles
800 to remove oxygen before inoculation with OD_{600} 0.1 *S. epidermidis* 1585 pTX*icaADBC*
801 overnight cultures grown in BHI/NaCl + 20 µg/mL tetracycline + 2% xylose. Control
802 experiments were designed to determine the function of iron containied in hemin in redox
803 transfer. We grew and treated *S. epidermidis* 1585 pTX*icaADBC* in similar conditions stated

above but replaced hemin with 5 µM protoporphyrin IX (PPIX) which had similar structure with hemin, but lacked iron. Electrodes were poised at 0.4 V and incubated at 37ºC. The potential induced biofilm formation on the electrode, using it as an electron acceptor in the absence of oxygen. Time-based electroanalyses (CA, DPV and charge measurements) were carried out on the growing biofilms for up to 120 h using parameters described above. Immunolabelling for time-based experiments, involved the use of different electrode set-ups for each time considered and immunolabeling and microscopy were subsequently conducted as described above.

Detection of G4-DNA/hemin peroxidase activity

The G4-DNA/hemin complex is also a DNAzyme with peroxidase-like activity. It could therefore also contribute to EET by transferring electrons to alternative electron acceptors, such as hydrogen peroxide (H_2O_2). We validated the peroxidase activity of the G4-DNA/hemin adsorbed to *S. epidermidis* 1585 pTX*icaADBC* using tyramide signal amplification (TSA). This method is commonly used in immunolabelling with horseradish peroxidase (HRP)-conjugated antibody. In our assay, we visualized the location of peroxidase activity stemming from the G4-DNA/hemin DNAzyme before proceeding to test if the DNAzyme can catalyse the transfer of electrons from bacteria to H_2O_2.

Overnight cultures of *S. epidermidis* 1585 pTX*icaADBC* were grown in BHI/NaCl supplemented with tetracycline (20 µg/ml), and xylose (2% w/v) and contained a combination of planktonic bacteria and larger aggregates. Twenty µL culture was transferred to an Eppendorf tube with a cut-off pipette tip to avoid shearing of the aggregates. Aggregates were suspended in 200 µL modified MES buffer adjusted to pH 6.5. Samples were supplemented with G4-DNA (5 µM) and/or hemin (5 µM) and vortexed for (30 s) before transferring 90 µL to a coverslip with an attached Gene Frame (Thermo Scientific, AB0577) and incubating for 30 min (RT, 50 rpm shaking) to let the bacteria and aggregates adsorb before removing the liquid and replacing it with 90 µL tyramide reagent containing tyramide conjugated with Alexa Fluor 488 (1:100) (Invitrogen, B40953), 2 mM ATP (Thermo Scientific, R0441), and 0.1% hydrogen peroxide (Sigma, 216763) in modified MES buffer. Samples were then incubated for 90 min (RT, 50 rpm). Samples were washed with modified MES buffer, and stained for 30 min (RT, 50 rpm), with 90 µL of 20 µM SYTO™ 60 (Invitrogen, S11342) prepared as 100 x aliquots in sterile deionized water. Samples were then mounted with Prolong™ Glass Antifade Mountant (Invitrogen, P3698) after a gentle wash before CLSM imaging as described above. Tyramide-AlexaFLour-488 was excited at 488 nm and emission detected from <550 nm. SYTO™ 60 was excited at 647 nm and emission detected at 650-700 nm. Both lasers were scanned in the same track with a beam splitter at 560 nm. Planktonic cells prepared as described above but not stained with Syto 60, were also used. Bright field images showed the planktonic cells during tyramide assay.

Electrochemical detection of residual hydrogen peroxide after degradation

After confirming peroxidase activity of the G4-DNA/hemin complex, we proceeded to determine if bacteria could transfer electrons from their metabolism to H_2O_2 via G4-DNA/hemin. We measured the capacity for bacteria to remove H_2O_2, comparing *S. epidermidis* 1585 pTX*icaADBC* in the presence or absence of hemin, G4-DNA or both.

Overnight cultures of *S. epidermidis* 1585 pTX*icaADBC* were prepared as described for the TSA assay, transferred to an Eppendorf tube, diluted to OD_{600} of 1 in fresh media and supplied with G4-DNA (5 µM) and/or hemin (5 µM). 200 µL culture was centrifuged (at 1118 × *g* for 2 min) and washed in same volume of 0.1 M KCl. Cells were resuspended in 200 µL modified MES buffer in 500 µL tubes and sparged with N_2 gas for 30 s before addition of 0.1% hydrogen peroxide and incubating at 37ºC with gentle shaking (40 rpm) for 5 min. After incubation,

854 cultures were centrifuged at 1118 × *g* for 2 min, and the supernatant was collected. The
855 supernatant (50 μL) was dropcast on sterile SPEs connected to potentiostat and cyclic
856 voltammetry was immediately run from 0.8 V to -0.8 V at 50 mV/s to detect H_2O_2. Buffer
857 containing undegraded 0.1% H_2O_2 served as the first control. G4-DNA (5 μM) mixed with
858 hemin (5 μM) in 200 μL modified MES buffer containing 0.1% H_2O_2 were incubated
859 anaerobically and used as a second control.
860
861

862 **EXTENDED DATA**
863
864
865

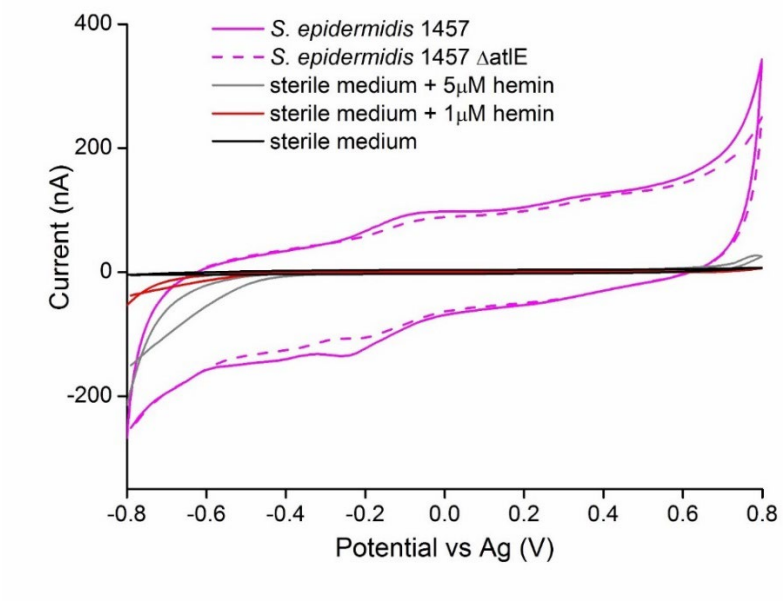

866
867 **Extended Data Fig. 1**: Cyclic Voltammogram (CV) of biofilms formed by *S. epidermidis* 1457
868 (eDNA producing) and *S. epidermidis* 1457 Δ*atlE* (autolysin deficient and low eDNA
869 producing) when grown with 5 μM hemin for 48 h. Sterile TSB/0.2 M NaCl medium and Sterile
870 medium (+1 μM and +5 μM hemin) served as controls.
871

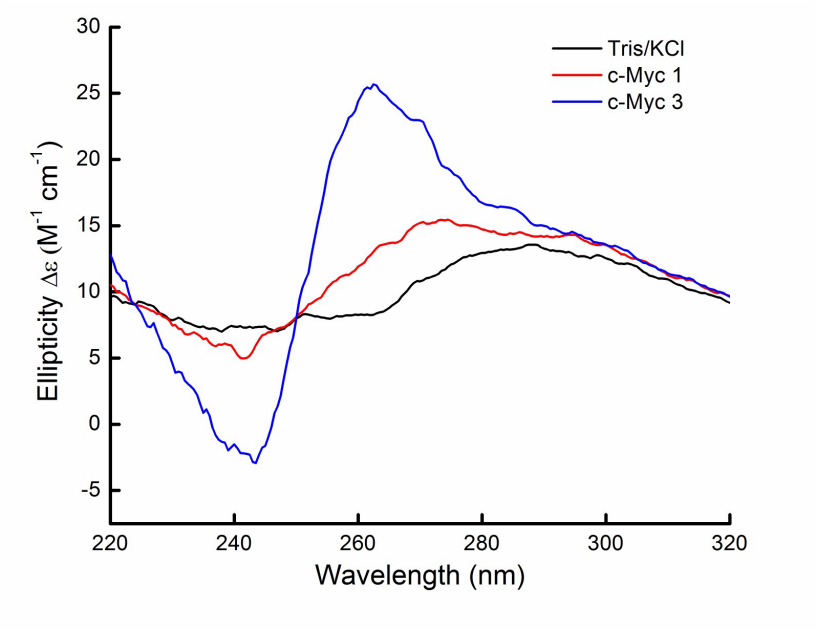

Extended Data Fig. 2: Circular dichroism confirms the structure of G4-DNA oligonucleotides

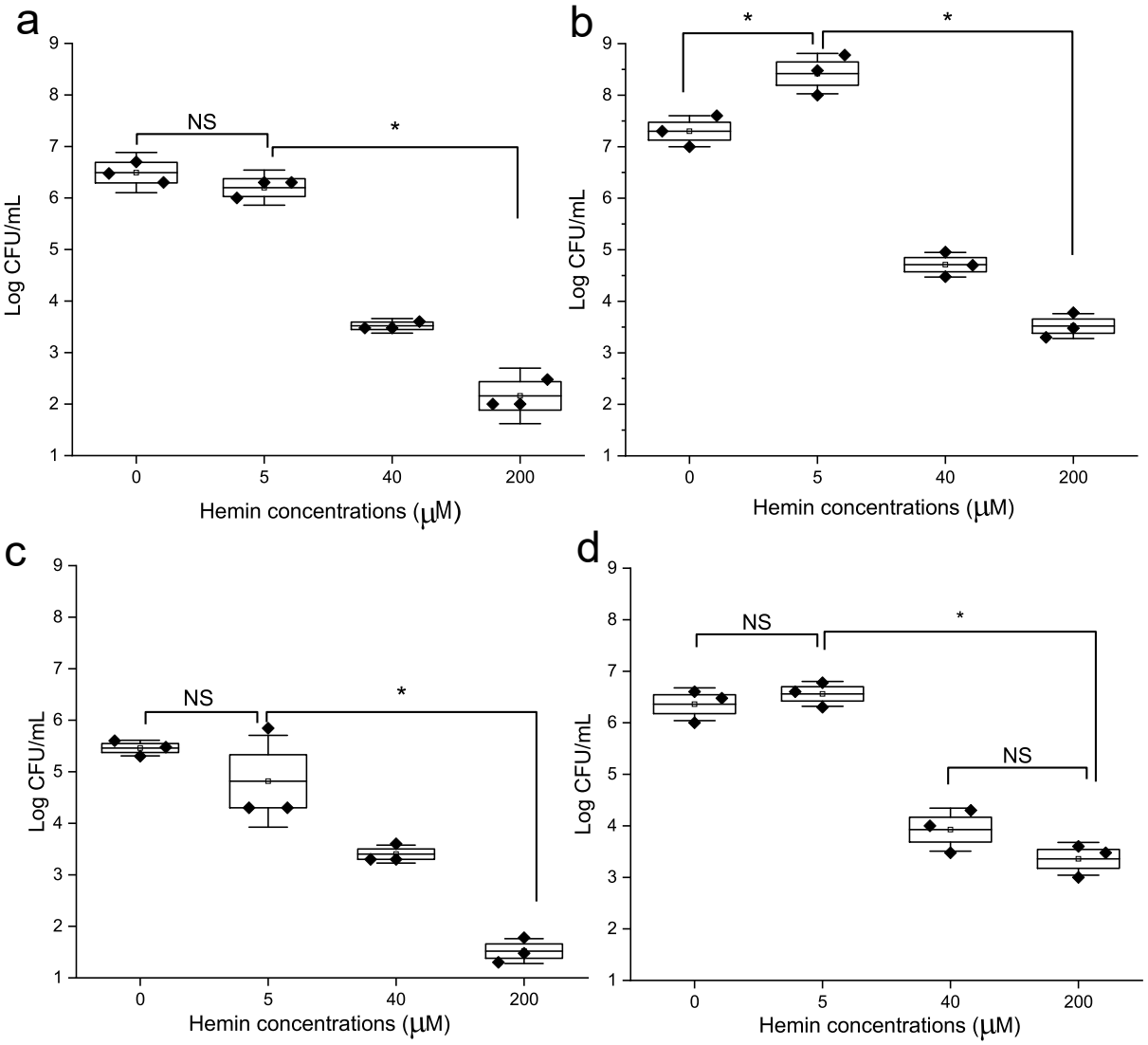

Extended Data Fig. 3: Cell viability and tolerance tests of planktonic cultures of *S. epidermidis* grown in varying concentrations of hemin with or without PNAG induction and G4-DNA (c-Myc3, 5 μM) addition (a) PNAG -, G4-DNA + (b) PNAG +,G4-DNA + (c) PNAG - , G4-DNA - (d) PNAG +, G4-DNA –. ∗ represents statistical significance ($p < 0.05$), ANOVA and Tukey's test, NS= Not significant.

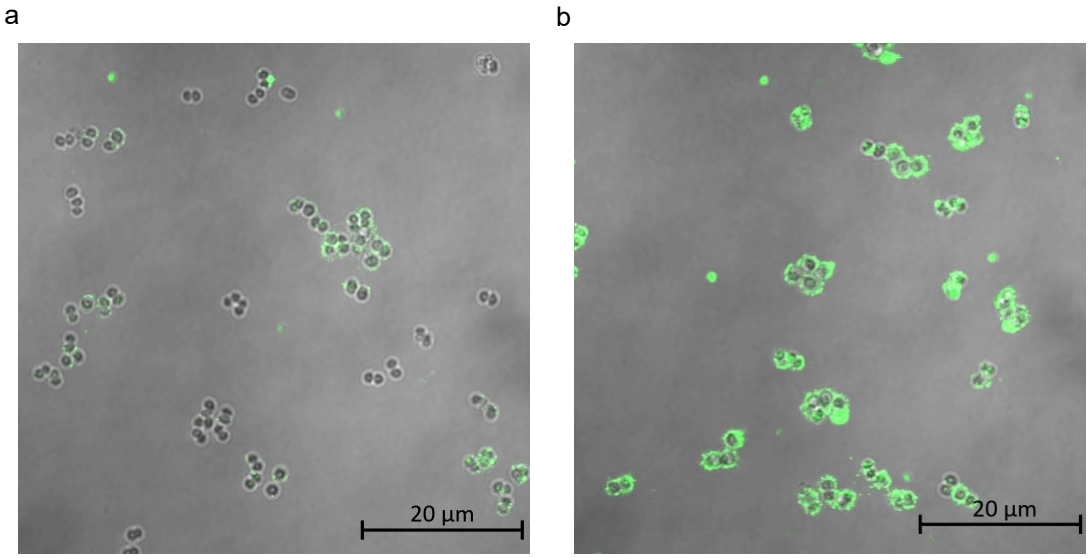

Extended Data Fig. 4: Adsorption of c-Myc1 (A) and c-Myc3 (B) to the surface of *S. epidermidis* with induced PNAG production. More G4-DNA was detected on the bacterial surface when using c-Myc3, and this oligo was therefore used in our subsequent experiments.

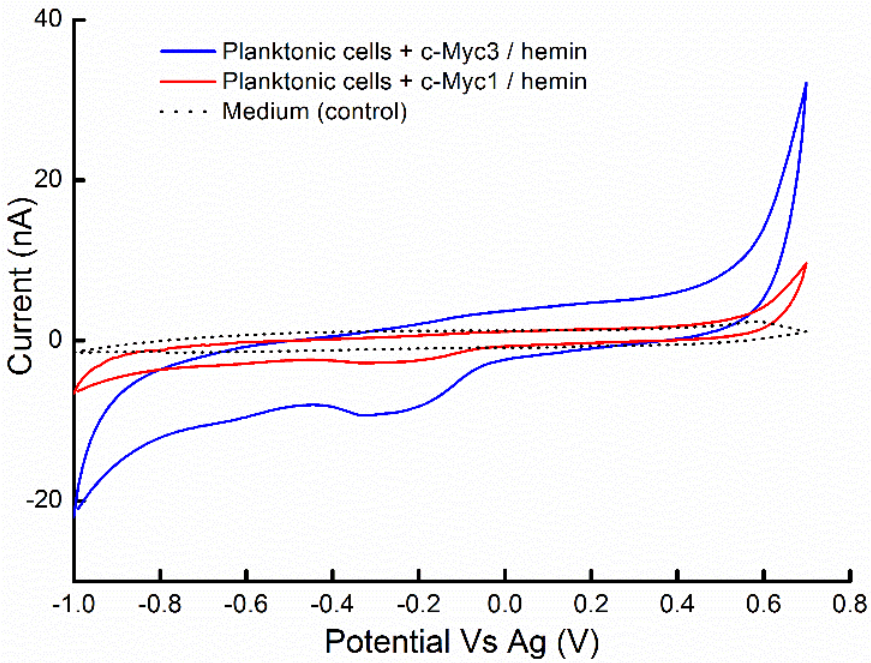

Extended Data Fig. 5: Cyclic Voltammogram (CV) shows that bacteria with c-Myc3 are more electroactive. Planktonic *S. epidermidis* were grown in TSB/NaCl with xylose (for PNAG production) and treated with 5 µM G4-DNA and 5 µM hemin before adsorption to the electrode and measurement of CV.

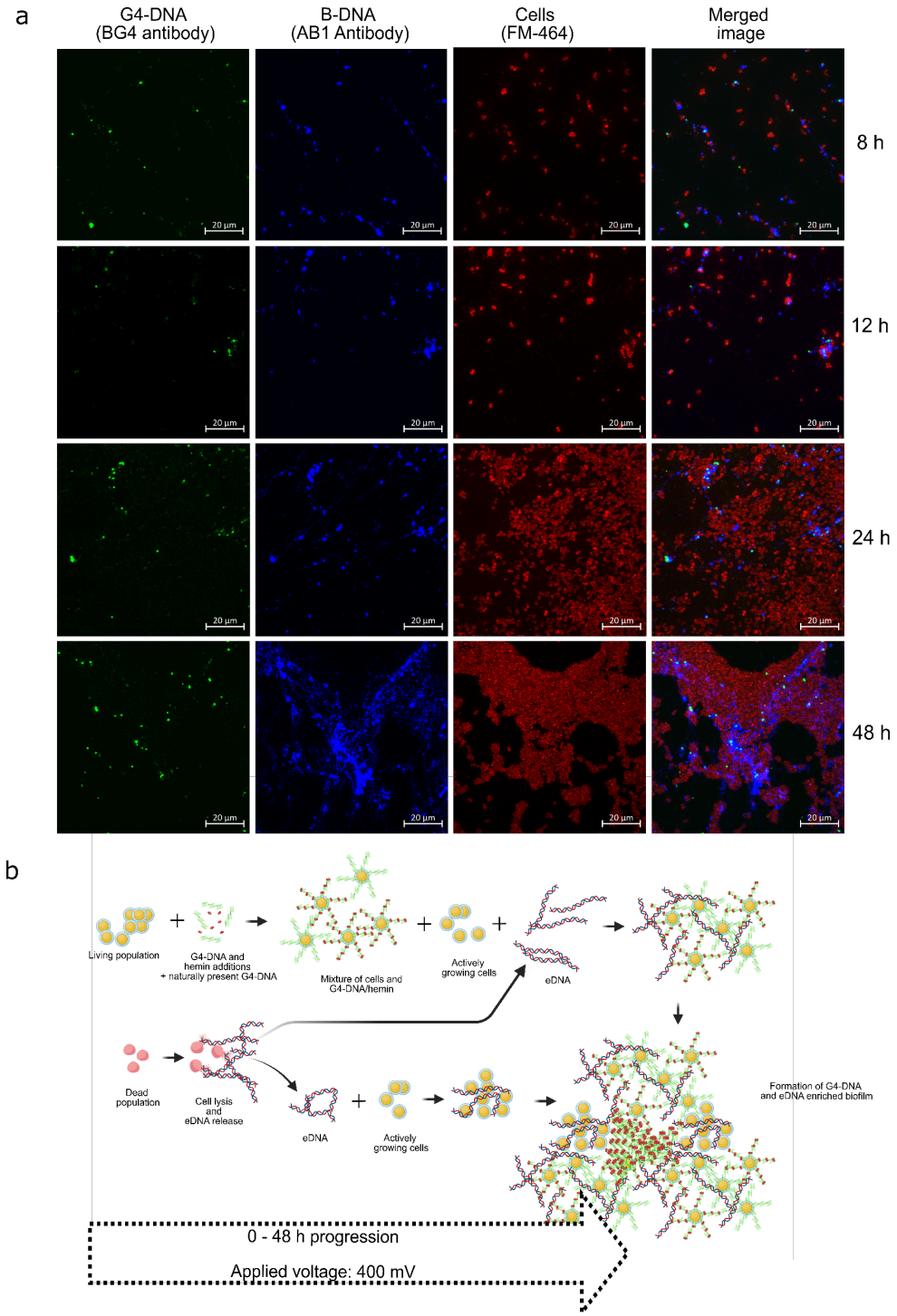

Extended Data Fig. 6: Externally added G4-DNA are gradually recruited over time by eDNA formed in the biofilm matrix. Time-based recruitment of free-floating G4-DNA for formation of enriched biofilm with G4-DNA/hemin complex under electrical influence of 0.4V poised potential (a) Microscopic observation of biofilm formation from 8h to 48h showing gradual G4-DNA incorporated over time into the biofilm under electrical influence (b) Proposed scheme for G4-DNA enriched biofilm formation over 48h. We propose that initial eDNA (presented as B-DNA) start to appear due to lysis of some cells from the starting inoculum after first exposure to applied electric potential. Gradual incorporation of G4-DNA into electroactive biomass leads to interactions between B-DNA and G4-DNA, as well as G4-DNA and cells. (b) is created in BioRender. Ajunwa, O. (2024) https://BioRender.com/h06f025

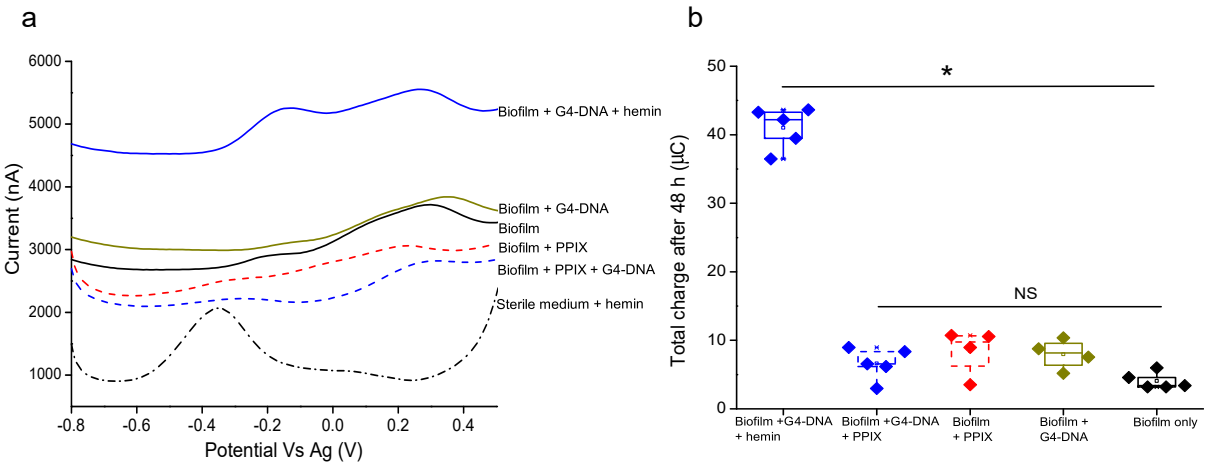

Extended Data Fig. 7: Biofilms grown with G4-DNA and hemin facilitate EET in an iron dependent fashion. Comparative electroactivity of 48 h old biofilms of *S. epidermidis* with induced PNAG production. Biofilms were supplemented with G4-DNA and either hemin or the iron deficient PPIX. (A) DPV shows PPIX treated biofilms lack the characteristic negative potential peak (-0.3 V to 0.1 V) associated with G4-DNA/hemin interactions (B) Total electric charge generated from biofilms also confirm the requirement of iron porphyrin to facilitate charge transfer (∗ represents significant difference ($p < 0.05$) based on ANOVA and Tukey's test, NS: Not significant).

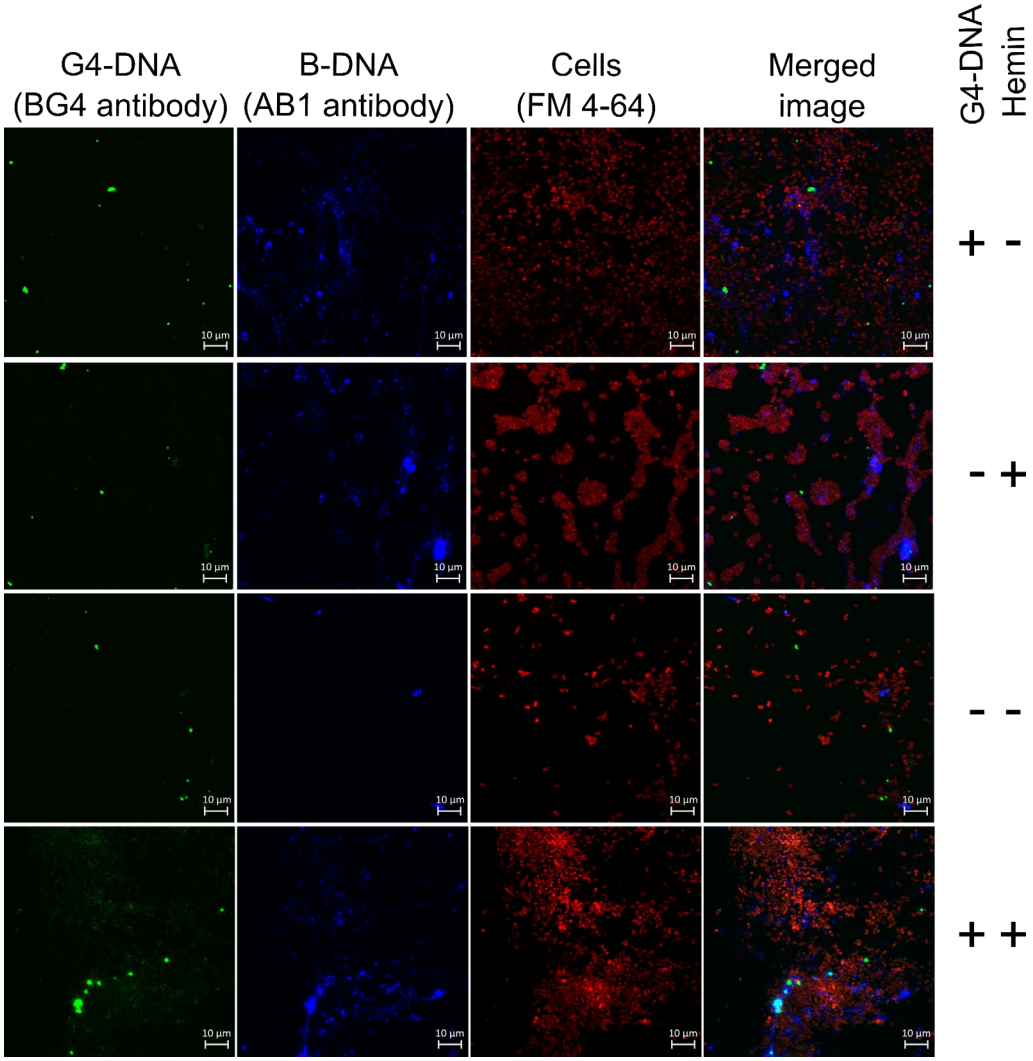

Extended Data Fig. 8. Representative microscopy images of *S. epidermidis* 1585 pTX*ica* biofilms formed on electrodes after 48 h with different treatments of G4-DNA (+/-) and hemin (+/-). Samples with both G4-DNA and hemin forms nodular structures of G4-DNA that associate with B-DNA in the biofilm.

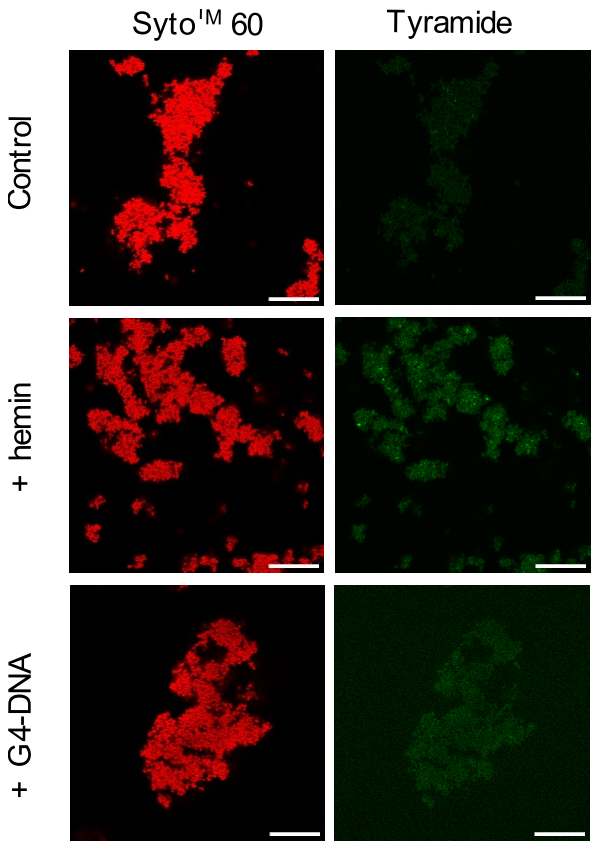

Extended Data Fig. 9. Lack of G4-DNA/hemin on the bacteria results in low peroxidase-like activity. Tyramide signal amplification shows low signals around the cells after reacting with tyramide and hydrogen peroxide. CLSM of bacterial aggregates stained by Syto 60 (red). Peroxidase activity showing minimal fluorescence at sites of peroxidase activity. Scale bar = 20 µm.